

University of Windsor
Scholarship at UWindsor

[Electronic Theses and Dissertations](#)

[Theses, Dissertations, and Major Papers](#)

9-16-2019

Estimation And Tracking Algorithm For Autonomous Vehicles And Humans

Jingyu Wang
University of Windsor

Follow this and additional works at: <https://scholar.uwindsor.ca/etd>

Recommended Citation

Wang, Jingyu, "Estimation And Tracking Algorithm For Autonomous Vehicles And Humans" (2019).
Electronic Theses and Dissertations. 7852.
<https://scholar.uwindsor.ca/etd/7852>

This online database contains the full-text of PhD dissertations and Masters' theses of University of Windsor students from 1954 forward. These documents are made available for personal study and research purposes only, in accordance with the Canadian Copyright Act and the Creative Commons license—CC BY-NC-ND (Attribution, Non-Commercial, No Derivative Works). Under this license, works must always be attributed to the copyright holder (original author), cannot be used for any commercial purposes, and may not be altered. Any other use would require the permission of the copyright holder. Students may inquire about withdrawing their dissertation and/or thesis from this database. For additional inquiries, please contact the repository administrator via email (scholarship@uwindsor.ca) or by telephone at 519-253-3000 ext. 3208.

**ESTIMATION AND TRACKING ALGORITHM FOR AUTONOMOUS
VEHICLES AND HUMANS**

by

Jingyu Wang

A Thesis
Submitted to the Faculty of Graduate Studies
through the Department of Electrical and Computer Engineering
in Partial Fulfilment of the Requirements for
the Degree of Master of Applied Science at the
University of Windsor

Windsor, Ontario, Canada

ESTIMATION AND TRACKING ALGORITHM FOR AUTONOMOUS
VEHICLES AND HUMANS

by
Jingyu Wang

APPROVED BY:

S. Das
Department of Civil and Environmental Engineering

X. Chen
Department of Electrical and Computer Engineering

B. Balasingam, Advisor
Department of Electrical and Computer Engineering

September 16, 2019

Declaration of Co-Authorship /

Previous Publication

Co-Authorship

I hereby declare that this thesis incorporates material that is result of joint research, as follows: Chapter 4 of this thesis was co-authored with R.K. Dhanapal and P. Ramakrishnan under the supervision of professor Balasingam. R.K. Dhanapal and P. Ramakrishnan contributed to the statistical analysis and graphing results. Chapter 5 of this thesis was co-authored with R.K. Dhanapal, P. Ramakrishnan, T. Silva and R. Maev under the supervision of professor Balasingam. R.K. Dhanapal and P. Ramakrishnan contributed to graphing results; T. Silva and R. Maev provided raw data. In all cases, the key ideas, primary contributions, experimental designs, data analysis, interpretation, and writing were performed by the author.

I am aware of the University of Windsor Senate Policy on Authorship and I certify that I have properly acknowledged the contribution of other researchers to my thesis, and have obtained written permission from each of the co-author(s) to include the above material(s) in my thesis.

Previous Publication

This thesis includes 2 original papers that have been previously submitted for publication in peer reviewed journals, as follows:

Thesis chapter	Publication title/full citation	Publication status
4	J. Wang, R.K. Dhanapal, P. Ramakrishnan, and B. Balasingam, “Quickest Detection of Abnormal Vehicle Movements on Highways,” 22nd International Conference on Information Fusion, Ottawa, Canada, 2019.	Accepted
5	J. Wang, R.K. Dhanapal, P. Ramakrishnan, and B. Balasingam, T. Silva, R. Maev “Active RFID Based Indoor Localization,” 22nd International Conference on Information Fusion, Ottawa, Canada, 2019	Accepted

I certify that I have obtained a written permission from the copyright owners to include the above published materials in my thesis. I certify that the above material describes work completed during my registration as a graduate student at the University of Windsor.

General

I declare that, to the best of my knowledge, my thesis does not infringe upon anyone's copyright nor violate any proprietary rights and that any ideas, techniques, quotations, or any other material from the work of other people included in my thesis, published or otherwise, are fully acknowledged in accordance with the standard referencing practices. Furthermore, to the extent that I have included copyrighted material that surpasses the bounds of fair dealing within the meaning of the Canada Copyright Act, I certify that I have obtained a written permission from the copyright owner(s) to include such material(s) in my thesis. I declare that this is a true copy

of my thesis, including any final revisions, as approved by my thesis committee and the Graduate Studies office, and that this thesis has not been submitted for a higher degree to any other University or Institution.

Abstract

Autonomous driving systems have experienced impressive growth in recent years. The present research community is working on several challenging aspects, such as, tracking, localization, path planning and control. In this thesis, first, we focus on tracking system and present a method to accurately track a moving vehicle. In the vehicle tracking, considering the proximity of surrounding vehicles, it is critical to detect their unusual maneuvers as quickly as possible, especially when autonomous vehicles operate among human-operated traffic. In this work, we present an approach to quickly detect lane-changing maneuvers of the nearby vehicles. The proposed algorithm is based on the optimal likelihood ratio test, known as Page test.

Second, we consider another form of tracking: tracking the movements of humans in indoor settings. Indoor localization of staff and patients based on radio frequency identification (RFID) technology has promising potential application in the healthcare sector. The use of an active RFID in real-time indoor positioning system without any sacrifice of localization accuracy is intended to provide security, guidance and support service to patients. In this paper maximum likelihood estimation along with its Cramer-Rao lower bound of the locations of active RFID tags are presented by exploring the received signal strength indicator which is collected at the readers. The performance of real-time localization system is implemented by using an extended Kalman filter (EKF).

Acknowledgements

First of all, I would like to express my gratitude to my parents who have raised me and provided endless help when I met the difficulties.

Second, I would like to extend my sincere gratitude to my supervisor, Dr. B. Balasingam who gave me an opportunity to transfer my major from Mechanical Engineering to Electrical Engineering and provided guidance on how to conduct research and beat obstacles. He is my first supervisor and the best one I have ever encountered. If possible, I would like to become a supervisor like him.

Further, I would also like to thank my committee members Dr. S. Das and Dr. X. Chen for their constructive comments and positive criticism.

I would like to express my gratitude to my friends who have always been helping me out of difficulties and supporting without a word of complaint.

Especially, I thank Andria Ballo for her help and support. Further I thank the fellow graduate students for their cooperation during the research period.

Contents

Declaration of Co-Authorship / Previous Publication	iii
Abstract	vi
List of Tables	xi
List of Figures	xii
1 Introduction	1
1.1 Autonomous Driving Sysyem	1
1.2 Challenges in Autonomous Driving	4
1.3 Object Tracking Algorithms	4
1.4 Indoor Localization with RFID	5
1.5 Organization	6
1.6 Bibliography	6
2 Kalman Filter for Tracking	8
2.1 Introduction	8
2.2 Tracking With Kalman Filter	9
2.2.1 The Estimation Algorithm	12
2.3 Tracking With Extended Kalman Filter	13
2.3.1 Derivation of the EKF	16
2.3.2 The First-Order EKF Algorithm	18

2.4	Bibliography	21
3	Page Test Algorithm	22
3.1	Introduction	22
3.2	Known Parameter After Change	23
3.2.1	CUSUM Algorithm	26
3.3	Unknown Parameter After Change	27
3.4	Bibliography	29
4	Quickest Detection of Abnormal Vehicle Movements on Highways	30
4.1	Introduction	30
4.2	Vehicle Motion Model on Highways	34
4.3	Review of Quickest Detection Algorithm	38
4.3.1	Problem Definition	38
4.3.2	Batch Detection	39
4.3.3	Recursive Detection	40
4.4	Fastest Detection of Non-Linear States	41
4.4.1	Fastest Detection of Lane Index (LIDX)	41
4.4.2	Fastest Detection of Lane-Change Index (LcIDX)	42
4.5	Simulation Results	44
4.5.1	Demonstration of Quickest Detection	45
4.5.2	Continuous Detection Algorithm	47
4.6	Conclusions	48
4.7	Bibliography	52
5	Active RFID Based Indoor Localization	58
5.1	Introduction	58
5.2	Problem Statement	61
5.3	Proposed Solution	65

5.3.1	Initialization through Maximum Likelihood Estimation	65
5.3.2	Estimate Environment Constant	68
5.3.3	Tracking	70
5.4	Cramer-Rao Lower Bound And Posterior Cramer-Rao Lower Bound .	70
5.5	Simulation Results	74
5.6	Conclusions	80
5.7	Bibliography	80
6	Conclusion and Future Work	83
Vita Auctoris		84

List of Tables

4.1 Number of Samples Before Contact (60 Hz)	36
--	----

List of Figures

1.1	Figure from a camera. An autonomous vehicle uses camera data to perceive objects in its environment [4].	2
1.2	An autonomous vehicle uses Radar to detect objects [4].	3
1.3	Measurements from a Velodyne Lidar. Lidar produces a set of data points that show nearby cars. Makers of self-driving car consider it essential tech [5].	3
2.4	Tracking with horizontal and vertical displacement	10
2.5	One cycle of the Kalman filter	13
2.6	Kalman filter tracking results	14
2.7	Tracking with distance and angle	15
2.8	Flow chart of the EKF	20
2.9	EKF tracking results. Distance and angle are converted to the Cartesian coordinates.	20
3.10	Measurements from the Gaussian distribution.	25
3.11	Log-likelihood ratio s_k . Typical behavior of the log-likelihood ratio s_k corresponding to a change in the mean.	26
3.12	Typical behavior of the CUSUM decision function g_k	28

4.13 Highway driving scenario. Multi-lane highway scenario is depicted in this figure where vehicle A uses its sensors to track the state of vehicle B. The lane number of B is denoted by L_k , where $L_k \in [-2, -1, 0, 1, 2]$ is relative to the lane in which A is travelling.	35
4.14 Simulated trajectories. The relative position of vehicle B is shown as it is perceived by vehicle A (see Figure 4.13). The trajectory of the vehicle center is plotted assuming that the vehicle moves along the center of the lane. The top plot shows three different lane-changing scenarios of B which was already in front of A; the plot at the bottom shows a scenario of vehicle B overtaking vehicle A.	46
4.15 Relative trajectory of the vehicle B	48
4.16 Overtaking scenario. Here, the relative position of vehicle B is shown as it is perceived by vehicle A (see Figure 4.13) as B overtakes A.	49
4.17 State diagram	50
4.18 Continuous Overtaking scenario. Here, the relative position of vehicle B is shown as it is perceived by vehicle A (see Figure 4.13) as B overtakes A, and comes back to the original lane.	51
5.19 An illustration of the problem. Approximate positions of the RFID sensors are shown. The objective is to track the people on the tracks based on the signals received at their wearable receivers.	62
5.20 Iterative approach to estimate the environment constant c. The EKF is summarized in Algorithm 1 and the LS approach to estimate the constant c is summarized in (5.130)-(5.133).	69

5.21 Grid search. Grid search is used to decide the initial guess of MLE. The search is implemented on the entire rectangular field rather than along the running path in order to ensure that the proposed technol- ogy can be portable to a new facility with fewer modifications to the algorithm.	75
5.22 Grid search and Newton-Raphson and CRLB. Grid search is used to initialize the Newton-Raphson method. It is shown that the performance of the Newton-Raphson method is as good as the CRLB that was derived in (5.149).	76
5.23 Estimation of the environmental constant c. The performance of estimating constant c for different initial value c_0 assumptions is shown.	76
5.24 EKF, PCRLB and $\mathbf{P}(k k)$ The MSE of the EKF performance is compared to PCRLB and $\mathbf{P}(k k)$ (5.159). It shows a clear advantage of the proposed EKF algorithm in challenging (noisy) scenarios.	77
5.25 Noise standard deviation $\sigma_w = 0.5$. True vs. estimated trajectory at low-noise scenario.	78
5.26 Noise standard deviation $\sigma_w = 0.8$. True vs. estimated trajectory for medium noise scenario.	78
5.27 Noise standard deviation $\sigma_w = 1.2$. True vs. estimated trajectory is shown for a high noise scenario.	79
5.28 Noise standard deviation $\sigma_w = 2$. True vs. estimated trajectory is shown for a very-high noise scenario.	79

Chapter 1

Introduction

1.1 Autonomous Driving Sysyem

Interest in autonomous driving dates back to as early as 1920s , when the first radio-controlled “American Wonder” was demonstrated on New York City streets [1]. In the subsequent decades, we see that the autonomous cars have come a long way. In the 1980s, a vision-guided autonomous vehicle was a milestone in the history of self driving cars [2]. Starting in 2009, Google began developing its self-driving car project, now called Waymo. By 2013, numerous companies including Ford, General Motors, BMW and others have started working on their own self-driving car technologies. In 2014, Tesla released the Autopilot self-driving system for Tesla Model S. At that time, Autopilot included semi-autonomous driving and parking capabilities. In the following years, Tesla continuously updated its Autopilot Hardware to achieve more self-driving functions, such as Auto Lane Change, Automatic Driving on Highways and Autosteer. It is predicted that the global autonomous driving market will grow up to 173.15 billion dollars by 2030 [3], the future of autonomous vehicles is an ambitious era of safe and comfortable transportation.

Advanced sensors are vital to the autonomous driving system. Todays self-driving

cars use several advanced sensors, such as, Lidar, Radar, camera, and ultrasonic sensor. Fig 1.1,1.2, 1.3 show some measurements from above sensors. These sensors fall into two categories: active and passive sensors. The active sensors can send out energy in the form of a wave and look for objects based upon the information that comes back. One example is Radar, which emits radio waves that are returned by reflective objects in the path of the beam. Unlike the active sensors, the passive sensors can only take in information from the environment without emitting a wave, such as a camera. With these sensors, the self driving car can perceive the surrounding environments. For example, by emitting invisible lasers at incredibly fast speeds, lidar sensors can paint a detailed 3D picture from the signals that bounce back instantaneously. These signals create “point clouds” that represent the vehicle’s surrounding environment to enhance safety and diversity of sensor data.

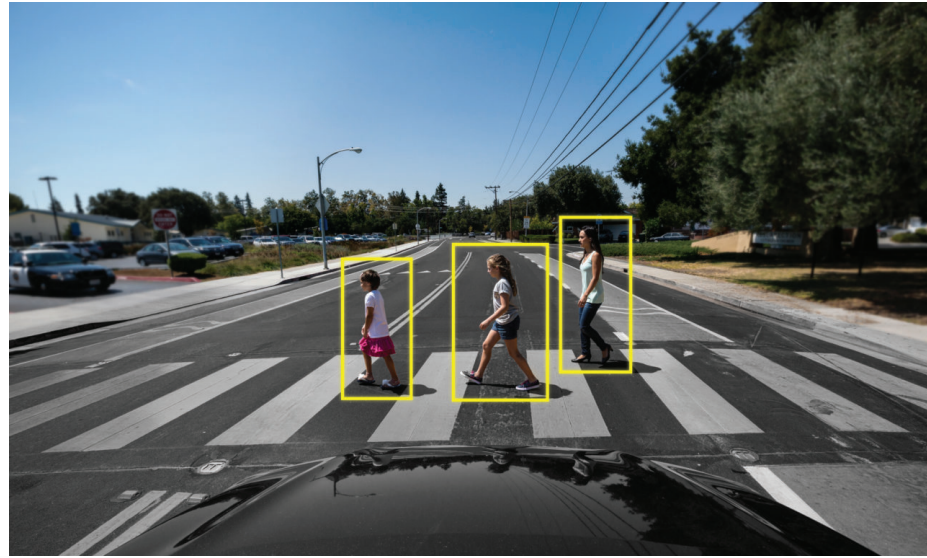


Figure 1.1: **Figure from a camera.** An autonomous vehicle uses camera data to perceive objects in its environment [4].

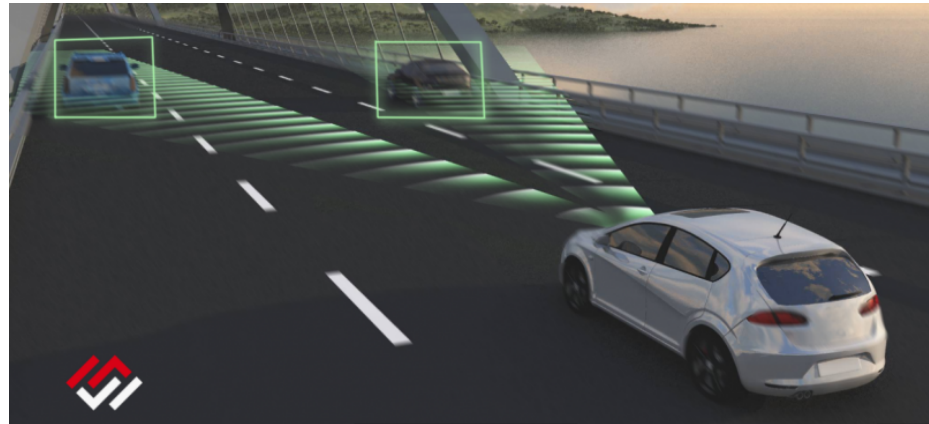


Figure 1.2: An autonomous vehicle uses Radar to detect objects [4].

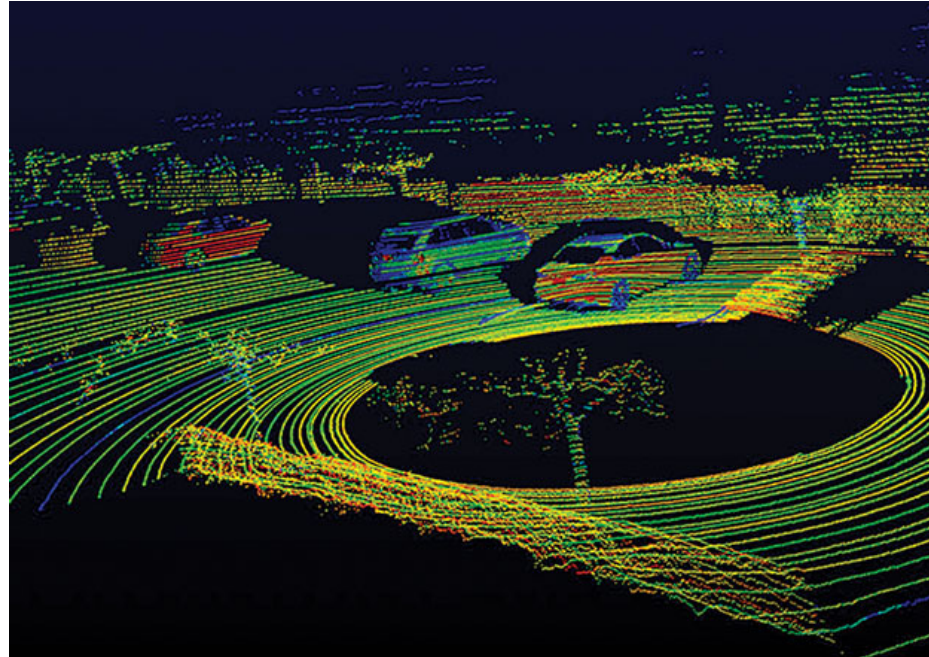


Figure 1.3: Measurements from a Velodyne Lidar. Lidar produces a set of data points that show nearby cars. Makers of self-driving car consider it essential tech [5].

1.2 Challenges in Autonomous Driving

Even though many companies are committed to launch their prototype self-driving cars by 2022, there are still some serious technical and safety challenges to overcome. First, self-driving cars still have a long way to go before they can safely handle bad weather conditions. For example, because the self-driving ability is relying heavily on the performance of a vehicle's cameras and other sensors, rain as well as snow will weaken sensors' performance and bring more noise to measurements.

Second, a far more difficult obstacle is the fact that driving is a highly social process that frequently involves complicated interactions with other drivers and pedestrians. In most of these situations, human drivers rely on human intelligence and common sense, whereas artificial intelligence still extremely lacks these abilities.

1.3 Object Tracking Algorithms

Object tracking is an important task among the field of autonomous driving. If the sensors (hardware) can be regarded as the body of the self driving car, then object tracking algorithms (software) are deemed to be the soul. In recent years, researchers have developed numerous algorithms. In 1986, TED J. Broida presented an approach for the estimation of object motion parameters from a sequence of noisy images [6]. By modeling the object dynamics as a function of time, this method can extract the estimates of the model parameters from the data using recursive techniques. To track efficiently in a multitarget, multimeasurement environment, the probabilistic multi-hypothesis tracking (PMHT) algorithm was proposed by RL Streit in 1995 [7]. In 2003, a mean shift algorithm was proposed by Q. Zhi to track the objects and their shape. [8]. In this thesis, we present the Page Test algorithm based on the likelihood ratio test to track the lane-changing information of the vehicles.

1.4 Indoor Localization with RFID

RFID (radio-frequency identification), which emits radio waves to wirelessly transmit the identity and other characteristics of an object, is an emerging localization technology that allows for tracking of objects or people. An RFID indoor tracking system typically consists of transponders (attached to objects), a reader and the data processing subsystem. In a passive RFID system, the reader acts as a power source and transfers energy to the transponder at short distance. The transponder draws power from it, energizes the embedded circuits and sends ID and data back to the reader. After that, these information is forwarded to the data processing system, where the data is processed.

As it only provides a limited tracking range of several meters, RFID is not suitable for outdoor localization. However, it is cost-effective, easy for maintenance and offers both identification and location. These advantages make tracking via RFID sensor especially suitable for hospital and industrial environments.

RFID localization has been an intensively researched topic in healthcare industry, driven by a greater emphasis on patient's safety than ever seen before. Some applications of RFID in the medical area are listed below.

1. Patient and staff tracking.
2. Tracking medicine and pharmaceuticals fast and accurately.
3. Trackig surgical tools and expensive equipment.
4. Access control (The staff members must wave or tap their RFID-enabled badges in front of door reader to gain access)

It is important for hospitals to have these information in order to effectively perform their stressful tasks. In this thesis, we present a method to find the received signal strength information (RSSI) based localization approach using active RFID system.

1.5 Organization

The remainder of this thesis is organized as follows. Chapter 2 introduces the fundamental of Kalman filter and Extended Kalman filter by using two vehicle tracking examples. In chapter 3, the Page Test algorithm is reviewed for lane change detection. Chapter 4 provides detailed description of the vehicle tracking algorithm and the Page Test application in lane change detection. The RFID indoor tracking algorithm is proposed in chapter 5. Finally, chapter 6 presents the thesis conclusion.

1.6 Bibliography

- [1] T. Sentinel, “Phantom auto’will tour city,” *Google News Archive, ed*, 1926.
- [2] C. Thorpe, M. H. Hebert, T. Kanade, and S. A. Shafer, “Vision and navigation for the carnegie-mellon navlab,” *IEEE Transactions on Pattern Analysis and Machine Intelligence*, vol. 10, no. 3, pp. 362–373, 1988.
- [3] I. Coppa, P. Woodgate, and Z. Mohamed-Ghouse, “Global outlook 2016: spatial information industry,” *Australia and New Zealand Cooperative Research Centre for Spatial Information, Melbourne*, 2016.
- [4] “How does a self-driving car see?: Nvidia blog,” Apr 2019. [Online]. Available: <https://blogs.nvidia.com/blog/2019/04/15/how-does-a-self-driving-car-see/>
- [5] E. Ackerman, “Cheap lidar: The key to making self-driving cars affordable,” *IEEE Spectrum*, vol. 22, 2016.
- [6] T. J. Broida and R. Chellappa, “Estimation of object motion parameters from noisy images,” *IEEE Transactions on Pattern Analysis & Machine Intelligence*, no. 1, pp. 90–99, 1986.

- [7] R. L. Streit and T. E. Luginbuhl, “Probabilistic multi-hypothesis tracking,” Naval Underwater Systems Center Newport RI, Tech. Rep., 1995.
- [8] Z.-Q. Wen and Z.-X. Cai, “Mean shift algorithm and its application in tracking of objects,” in *2006 International Conference on Machine Learning and Cybernetics*. IEEE, 2006, pp. 4024–4028.

Chapter 2

Kalman Filter for Tracking

2.1 Introduction

Given the measurements $z(k)$, $k=1, 2, 3, \dots$ how to get an accurate estimate of the target state $x(k)$? The best answer to this question was derived by R.E. Kalman in 1960 [2]. Kalman filter is a commonly used state estimation algorithm for linear system which provides a means of recursively estimating a parameter (or parameters). Because of its superior ability to extract the required information from noisy signal and its small computational and memory requirements, it is used in many application areas including spacecraft navigation, motion planning in robotics, and signal processing [3]. For nonlinear system, SJ Julier presented the Extended Kalman filter(EKF) in 1997 [1]. Although Kalman filter and EKF have relatively simple steps and require small computational resource, they are still not easy for people who are not familiar with estimation theory to understand and implement these algorithms. Thus this chapter will provide a basic understanding of Kalman filter and EKF, and give some examples to help understand them.

This chapter will be organized as follows: section 2.2 offers brief tutorials and an example on the Kalman filter, respectively. Section 2.3 provides a detailed description on the Extended Kalman filter.

2.2 Tracking With Kalman Filter

To use the Kalman filter for tracking the moving targets, it is necessary to design a dynamic model of target motion. The most common used model is a constant velocity (CV) model, which assumes that the velocity is constant during a sampling time [4]. This model has been used in many applications because of its versatility, effectiveness, and simplicity [4]. In this section, we will use the CV model to track the object.

Assuming there is a vehicle (vehicle A) with several sensors such as Radar and camera moving on the road. With these sensors, the vehicle A can obtain the horizontal and vertical displacements of a nearby vehicle (vehicle B) is depicted in Fig 2.4. We want to track the vehicle B and compute its trajectory using Kalman filter. The target's state can be represented as

$$\mathbf{x}(k) = [x(k) \quad \dot{x}(k) \quad y(k) \quad \dot{y}(k)]^T \quad (2.1)$$

where x and y denote the horizontal and vertical displacement from a reference point and \dot{x} and \dot{y} denote the velocity in the respective directions. The dynamic equation of the movement of the vehicle is given by

$$\mathbf{x}(k+1) = \mathbf{F}\mathbf{x}(k) + \mathbf{B}v(k) \quad (2.2)$$

where the process noise $v(k)$ is assumed zero-mean white/ The state transition matrix \mathbf{F} is

$$\mathbf{F} = \begin{bmatrix} 1 & T & 0 & 0 \\ 0 & 1 & 0 & 0 \\ 0 & 0 & 1 & T \\ 0 & 0 & 0 & 1 \end{bmatrix} \quad (2.3)$$

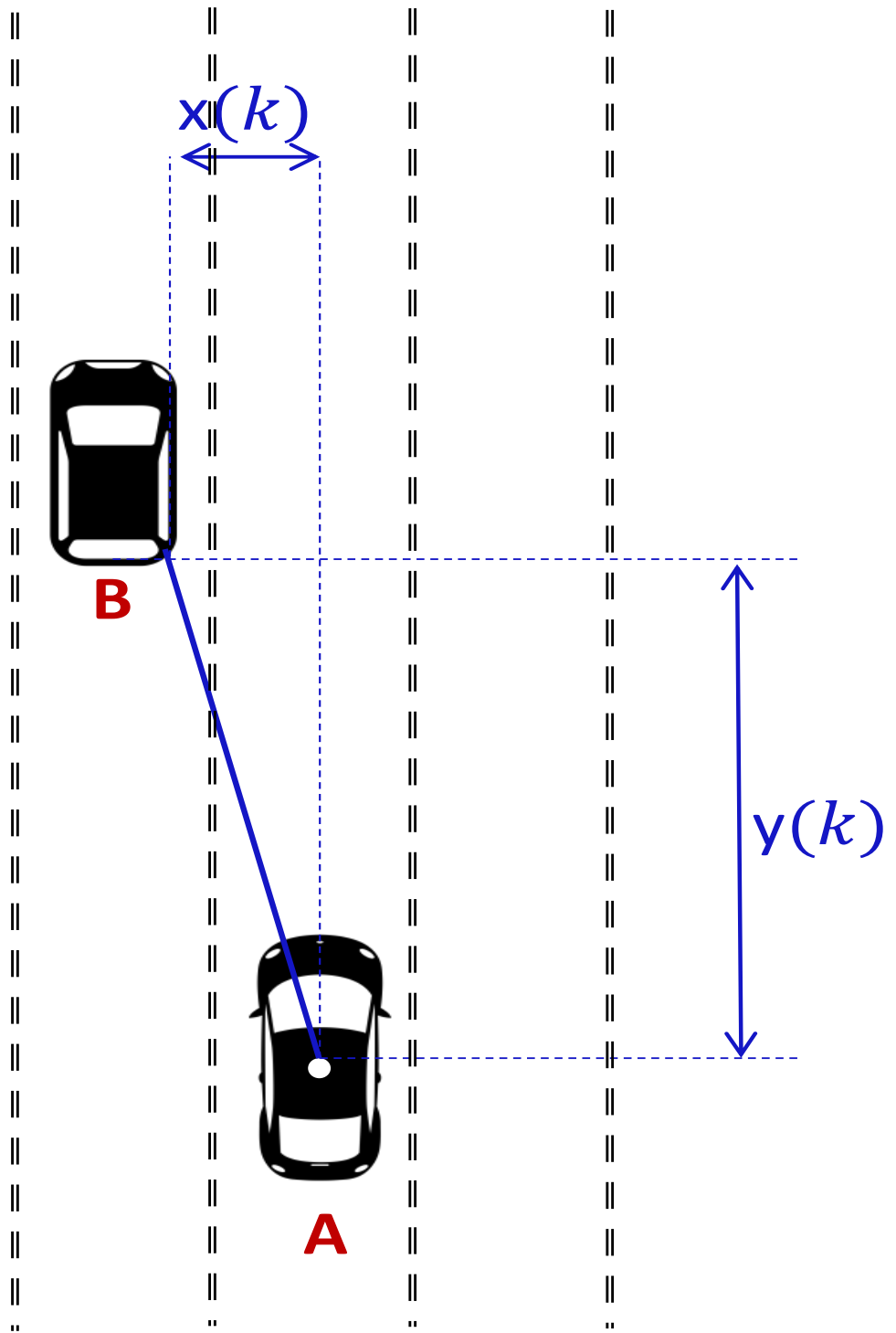


Figure 2.4: Tracking with horizontal and vertical displacement

where the sampling time T is 0.1s, and the vector gain \mathbf{B} multiplying the scalar process noise is given by

$$\mathbf{B} = \begin{bmatrix} \frac{1}{2}T^2 & 0 \\ T & 0 \\ 0 & \frac{1}{2}T^2 \\ 0 & T \end{bmatrix} \quad (2.4)$$

Then the covariance of the process multiplied by the gain, $\mathbf{B}v(k)$, is

$$\begin{aligned} \mathbf{Q} &= E[\mathbf{B}\mathbf{v}(k)(\mathbf{v}(k)\mathbf{B})'] = \mathbf{B}E[\mathbf{v}(k)\mathbf{v}(k)']\mathbf{B}^T = \mathbf{B}\sigma_v^2\mathbf{B}^T \\ &= \begin{bmatrix} \frac{1}{4}T^4 & \frac{1}{2}T^3 & 0 & 0 \\ \frac{1}{2}T^3 & T^2 & 0 & 0 \\ 0 & 0 & \frac{1}{4}T^4 & \frac{1}{2}T^3 \\ 0 & 0 & \frac{1}{2}T^3 & T^2 \end{bmatrix} \sigma_v^2 \end{aligned} \quad (2.5)$$

The state $\mathbf{x}(k)$ is observed through the measurement model \mathbf{H} as follows.

$$\mathbf{z}(k) = \mathbf{H}\mathbf{x}(k) + \mathbf{w}(k) \quad (2.6)$$

where

$$\mathbf{H} = \begin{bmatrix} 1 & 0 & 0 & 0 \\ 0 & 0 & 1 & 0 \end{bmatrix} \quad (2.7)$$

and $\mathbf{w}(k)$ is the measurement noise that is assumed to be Gaussian with covariance

$$\mathbf{R} = E[\mathbf{w}(k)\mathbf{w}(k)'] = \begin{bmatrix} \sigma_w^2 & 0 \\ 0 & \sigma_w^2 \end{bmatrix} \quad (2.8)$$

2.2.1 The Estimation Algorithm

As the dynamic model we mentioned before, the corresponding Kalman filter starts with the initial estimate $\hat{\mathbf{x}}(0|0)$ of $\mathbf{x}(0)$ and the associated initial covariance $\mathbf{P}(0|0)$.

One cycle of the Kalman filter has the following steps.

1. State Prediction

$$\hat{\mathbf{x}}(k+1|k) = \mathbf{F}\hat{\mathbf{x}}(k|k) \quad (2.9)$$

$$\mathbf{P}(k+1|k) = \mathbf{F}\mathbf{P}(k|k)\mathbf{F}' + \mathbf{Q}(k) \quad (2.10)$$

2. Measurement Prediction

$$\hat{\mathbf{z}}(k+1|k) = \mathbf{H}\hat{\mathbf{x}}(k+1|k) \quad (2.11)$$

$$\mathbf{S}(k+1) = \mathbf{H}\mathbf{P}(k+1|k)\mathbf{H}' + \mathbf{R}(k+1) \quad (2.12)$$

$$\mathbf{v}(k+1) = \mathbf{z}(k+1) - \hat{\mathbf{z}}(k+1|k) \quad (2.13)$$

3. Filter Gain

$$\mathbf{W}(k+1) = \mathbf{P}(k+1|k)\mathbf{H}'\mathbf{S}(k+1)^{-1} \quad (2.14)$$

4. State Update

$$\hat{\mathbf{x}}(k+1|k+1) = \hat{\mathbf{x}}(k+1|k) + \mathbf{W}(k+1)\mathbf{v}(k+1) \quad (2.15)$$

$$\mathbf{P}(k+1|k+1) = \mathbf{P}(k+1|k) - \mathbf{W}(k+1)\mathbf{S}(k+1)\mathbf{W}(k+1)' \quad (2.16)$$

The flow chart of one cycle of the Kalman filter is presented in Fig. 2.5 . Note that at every cycle k the entire past is summarized by the sufficient statistic $\hat{\mathbf{x}}(k|k)$ and the associated covariance $\mathbf{P}(k|k)$.

Fig 2.6 shows the tracking results by using Kalman filter.

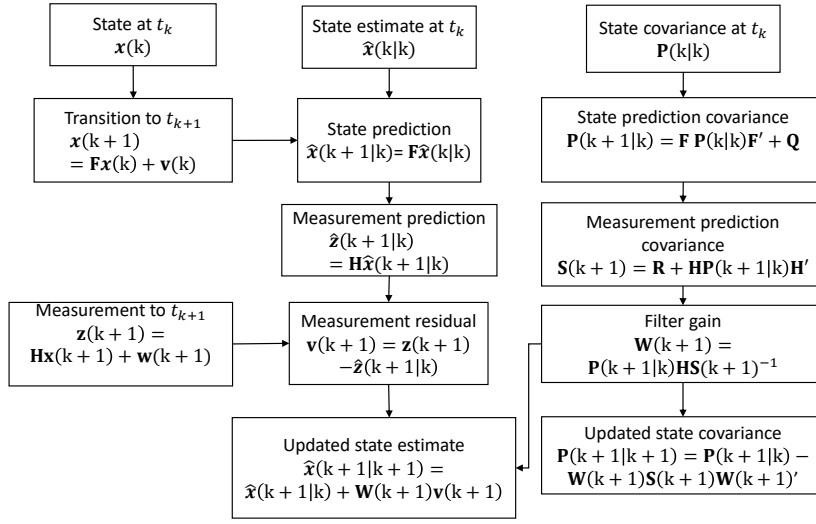


Figure 2.5: One cycle of the Kalman filter

2.3 Tracking With Extended Kalman Filter

The standard Kalman filter is used for linear system, whereas under non-linear system, the extended Kalman filter (EKF) is used. The EKF is designed to get the approximate estimation for a non-linear system. It can be obtained by a series expansion of the non-linear dynamics and of the measurement equations. The first order EKF is based on the linearization (first order series expansion of the nonlinearities)

Similarly, assuming there is a vehicle (vehicle A) with several sensors such as Radar and camera moving on the road. In this scenario, the vehicle A can obtain the distance and angle rather than the horizontal and vertical displacements of a nearby vehicle (vehicle B) is depicted in fig 2.7. In the present scenario, the target's state and dynamic equation are the same as equation 2.1 and 2.2, respectively. However, the measurement state vector is different which is given by

$$\mathbf{z}(k) = [d(k) \quad \theta(k)]^T \quad (2.17)$$

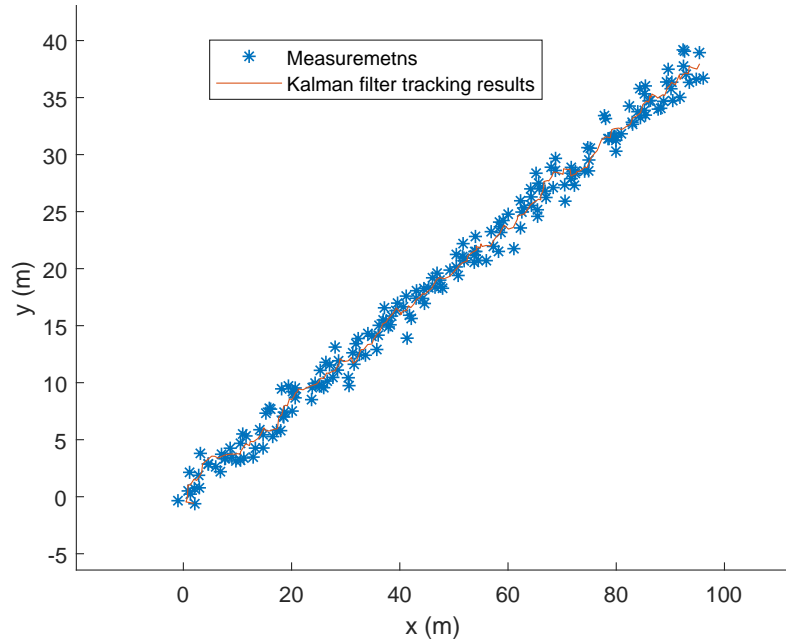


Figure 2.6: **Kalman filter tracking results**

and the measurement equation is

$$\mathbf{z}(k) = \mathbf{h}[\mathbf{x}(k)] + \mathbf{w}(k) \quad (2.18)$$

where $\mathbf{h}[\mathbf{x}(k)]$ is

$$\begin{bmatrix} \sqrt{x^2(k) + y^2(k)} \\ \arctan \frac{y(k)}{x(k)} \end{bmatrix} \quad (2.19)$$

The Jacobians of vector 2.19 is

$$\mathbf{H}(k) = \begin{bmatrix} \frac{x(k)}{\sqrt{x^2(k)+y^2(k)}} & 0 & \frac{y(k)}{\sqrt{x^2(k)+y^2(k)}} & 0 \\ -\frac{y(k)}{x^2(k)+y^2(k)} & 0 & \frac{x(k)}{x^2(k)+y^2(k)} & 0 \end{bmatrix} \quad (2.20)$$

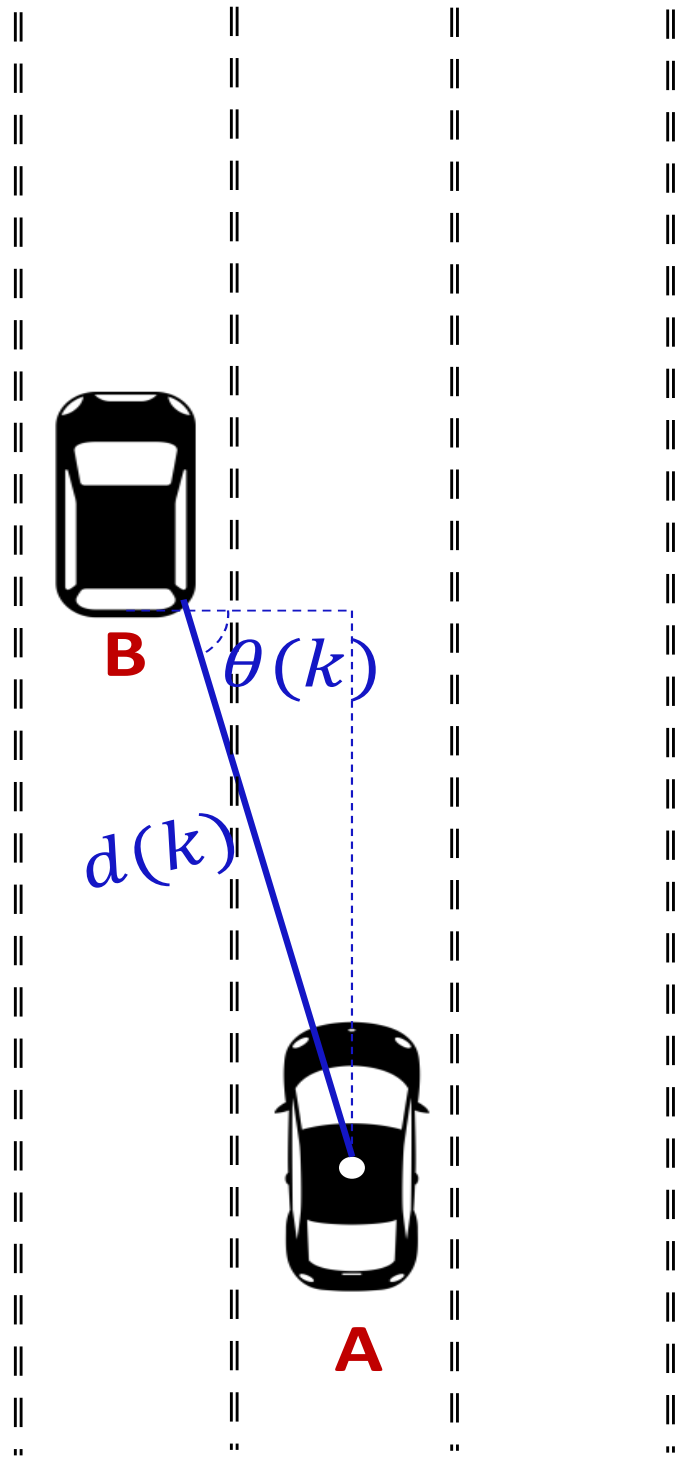


Figure 2.7: Tracking with distance and angle

and $\mathbf{w}(k)$ is the measurement noise with covariance

$$E[\mathbf{w}(k)\mathbf{w}(k)'] = \begin{bmatrix} \sigma_d^2 & 0 \\ 0 & \sigma_\theta^2 \end{bmatrix} \quad (2.21)$$

2.3.1 Derivation of the EKF

Consider a discrete-time non-linear dynamic system as follows:

The dynamic equation is

$$\mathbf{x}(k+1) = f[k, \mathbf{x}(k)] + \mathbf{v}(k) \quad (2.22)$$

where the noise $\mathbf{v}(k)$ is assumed additive, zero mean, and white

$$E[\mathbf{v}(k)] = 0 \quad (2.23)$$

$$E[\mathbf{v}(k)\mathbf{v}(j)'] = \mathbf{Q}(k)\delta_{kj} \quad (2.24)$$

The measurement equation is

$$\mathbf{z}(k) = h[k, \mathbf{x}(k)] + w(k) \quad (2.25)$$

where the measurement noise is additive, zero mean, and white

$$E[\mathbf{w}(k)] = 0 \quad (2.26)$$

$$E[\mathbf{w}(k)\mathbf{w}(j)'] = \mathbf{R}(k)\delta_{kj} \quad (2.27)$$

Consider a more general discrete-time non-linear dynamic model (The process model and the measurement model are both non-linear.) , whereas in the proposed example, only the measurement model is non-linear.

The dynamic equation is

$$\mathbf{x}(k+1) = f[k, \mathbf{x}(k)] + \mathbf{v}(k) \quad (2.28)$$

where the noise $\mathbf{v}(k)$ is assumed additive, zero mean, and white

$$E[\mathbf{v}(k)] = 0 \quad (2.29)$$

$$E[\mathbf{v}(k)\mathbf{v}(j)'] = \mathbf{Q}(k)\delta_{kj} \quad (2.30)$$

The measurement equation is

$$\mathbf{z}(k) = h[k, \mathbf{x}(k)] + w(k) \quad (2.31)$$

where the measurement noise is additive, zero mean, and white

$$E[\mathbf{w}(k)] = 0 \quad (2.32)$$

$$E[\mathbf{w}(k)\mathbf{w}(j)'] = \mathbf{R}(k)\delta_{kj} \quad (2.33)$$

To get the predicted state $\hat{\mathbf{x}}(k+1|k)$, the nonlinear function in (2.28) is expanded in the first-order Taylor series around the latest estimate $\hat{\mathbf{x}}(k|k)$. The vector Taylor series expansion is

$$\mathbf{x}(k+1) = f[k, \mathbf{x}(k)] + f_x(k)[\mathbf{x}(k) - \hat{\mathbf{x}}(k|k)] + HOT + \mathbf{v}(k) \quad (2.34)$$

where

$$f_x(k) \triangleq [\nabla_{\mathbf{x}}]f(k, \mathbf{x})'|_{\mathbf{x}=\hat{\mathbf{x}}(k|k)} \triangleq \frac{\partial f}{\partial \mathbf{x}} \quad (2.35)$$

is the Hessian of the vector f and HOT represents the higher-order terms, which will

be neglected. Given the data \mathbf{Z}^k , the above Jacobian is known. Thus predicted state to time $k+1$ from time k is obtained by taking the expectation of (2.34) conditioned on \mathbf{Z}^k and neglecting the HOT term.

$$\mathbf{x}(k+1) = f[k, \mathbf{x}(k)] \quad (2.36)$$

and the state prediction covariance is

$$\mathbf{P}(k+1|k) = f_x(k)\mathbf{P}(k|k)f_x(k)' \quad (2.37)$$

Similarly, the first-order predicted measurement is

$$\hat{\mathbf{z}}(k+1|k) = h[k+1, \hat{\mathbf{x}}(k+1|k)] \quad (2.38)$$

and the measurement prediction covariance is

$$\mathbf{S}(k+1) = h_x(k+1)\mathbf{P}(k+1|k)h_x(k+1)' \quad (2.39)$$

where the Jacobian of h is

$$h_x(k+1) \triangleq [\nabla_{\mathbf{x}}]h(k+1, \mathbf{x})'|_{\mathbf{x}=\hat{\mathbf{x}}(k+1|k)} \triangleq \frac{\partial h}{\partial \mathbf{x}} \quad (2.40)$$

2.3.2 The First-Order EKF Algorithm

The EKF also starts with the initial estimate $\hat{\mathbf{x}}(0|0)$ of $\mathbf{x}(0)$ and the associated initial covariance $\mathbf{P}(0|0)$. The one cycle of the EKF is listed below:

1. Evaluation of Jacobians

$$\mathbf{F}(k) = \frac{\partial f(k)}{\partial x}|_{\mathbf{x}=\hat{\mathbf{x}}(k|k)} \quad (2.41)$$

$$\mathbf{H}(k+1) = \frac{\partial h(k+1)}{\partial x}|_{\mathbf{x}=\hat{\mathbf{x}}(k+1|k)} \quad (2.42)$$

2. State Prediction

$$\hat{\mathbf{x}}(k+1|k) = f[k, \hat{\mathbf{x}}(k|k)] \quad (2.43)$$

$$\mathbf{P}(k+1|k) = \mathbf{F}(k)\mathbf{P}(k|k)\mathbf{F}(k)' + \mathbf{Q}(k) \quad (2.44)$$

3. Measurement Prediction

$$\hat{\mathbf{z}}(k+1|k) = h[k+1, \hat{\mathbf{x}}(k+1|k)] \quad (2.45)$$

$$\mathbf{S}(k+1) = \mathbf{H}(k+1)\mathbf{P}(k+1|k)\mathbf{H}(k+1)' + \mathbf{R}(k+1) \quad (2.46)$$

$$\mathbf{v}(k+1) = \mathbf{z}(k+1) - \hat{\mathbf{z}}(k+1|k) \quad (2.47)$$

3. Filter Gain

$$\mathbf{W}(k+1) = \mathbf{P}(k+1|k)\mathbf{H}(k+1)'\mathbf{S}(k+1)^{-1} \quad (2.48)$$

4. State Update

$$\hat{\mathbf{x}}(k+1|k+1) = \hat{\mathbf{x}}(k+1|k) + \mathbf{W}(k+1)\mathbf{v}(k+1) \quad (2.49)$$

$$\mathbf{P}(k+1|k+1) = \mathbf{P}(k+1|k) - \mathbf{W}(k+1)\mathbf{S}(k+1)\mathbf{W}(k+1)' \quad (2.50)$$

The flow chart of one cycle of the EKF is presented in fig. 2.8. Fig 2.9 shows the tracking results by using EKF.

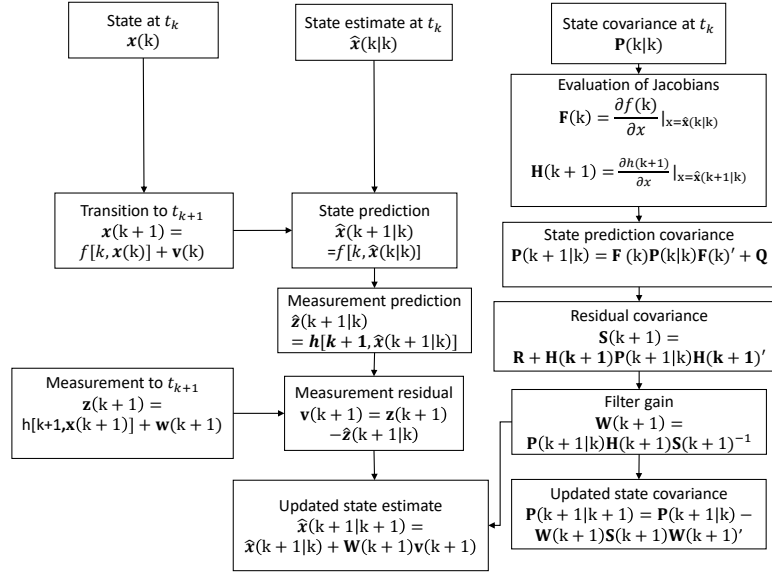


Figure 2.8: Flow chart of the EKF

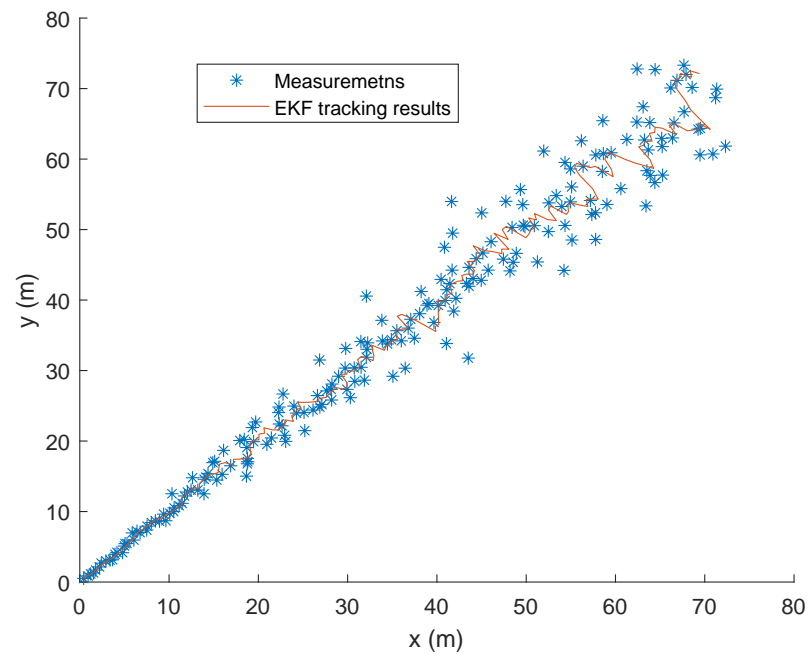


Figure 2.9: EKF tracking results. Distance and angle are converted to the Cartesian coordinates.

2.4 Bibliography

- [1] S. J. Julier and J. K. Uhlmann, “New extension of the kalman filter to nonlinear systems,” in *Signal processing, sensor fusion, and target recognition VI*, vol. 3068. International Society for Optics and Photonics, 1997, pp. 182–193.
- [2] R. E. Kalman, “A new approach to linear filtering and prediction problems,” *Journal of basic Engineering*, vol. 82, no. 1, pp. 35–45, 1960.
- [3] Y. Pei, S. Biswas, D. S. Fussell, and K. Pingali, “An elementary introduction to kalman filtering,” *arXiv preprint arXiv:1710.04055*, 2017.
- [4] K. Saho, “Kalman filter for moving object tracking: Performance analysis and filter design,” in *Kalman Filters-Theory for Advanced Applications*. IntechOpen, 2017.

Chapter 3

Page Test Algorithm

3.1 Introduction

An intensively investigated field is time series analysis and identification. Most of the theories underlying these investigations are the properties or parameter describing the measurements are either constant or slowly time-varying [1]. On the other hand, many practical problems are arising in recognition-oriented signal processing, fault detection and monitoring in navigation system, which can be regarded as a problem that the parameters are subject to abrupt changes at unknown time instants.

However, because most of the research in this field is aimed at solving slow changes problem, the detection of abrupt changes has been a problem of interest in many applications. In present days, there are so many sensors that constantly monitor the environment. The changes in their values happens in a frequent manner. For example, navigation systems are typical equipments for planes, warships, cars, and other moving objects. The inertial navigation system is an important part of the navigation system, which includes two types of sensors: gyros and accelerometers. Using these sensors and the dynamic motion equations, the estimation of the coordinates and the velocity can be obtained. To meet the safety and accuracy requirements, redundant fault-tolerant measurement systems are used to again quick detection and few false

alarms. Fast detection is necessary because, between the faulty onset time and the detection time, we use abnormal measurements in the navigation equations, which is highly unwanted. On the other hand, false alarms bring lower accuracy because some incorrect information is used. Therefore, the optimal solution is again a tradeoff between fast detection and false alarms [1].

Similiarly, the detection of abrupt changes is also useful in the self-driving technology, such as lane change detection and collision warning system, which only give us a few seconds to response. We therefore analyzed the lane change detection problem, and proposed the Page Test algorithm to deal with the abrupt lane change detection.

This chapter will be organized as follows: section 3.2 provides a known parameter after change Page Test algorithm, and in section 3.3, we developed the unknown parameter after change algorithm.

3.2 Known Parameter After Change

Firstly, we introduce the initial idea used in Page Test algorithm. Samples with fixed size N are taken, and at the end of the sample set a decision rule is computed to test between the two following hypotheses of the parameter θ

$$\begin{aligned} \mathbf{H}_0 & : \theta = \theta_0 \\ \mathbf{H}_1 & : \theta = \theta_1 \end{aligned} \tag{3.51}$$

If \mathbf{H}_0 is accepted, the sampling and test continue, otherwise sampling is stopped after the first sample of observations for which the decision is taken in favor of \mathbf{H}_1 .

Next, let

$$S_j^k = \sum_{i=j}^k s_i \tag{3.52}$$

where

$$s_i = \ln \frac{p_{\theta_1}(y_i)}{p_{\theta_0}(y_i)} \quad (3.53)$$

The following statement can be obtained directly from the Neyman-Pearson lemma [2]. For a fixed sample size N, the optimal decision rule d is given by

$$d = \begin{cases} 0 & \text{if } S_1^N < h; \mathbf{H}_0 \text{ is chosen} \\ 1 & \text{if } S_1^N \geq h; \mathbf{H}_1 \text{ is chosen} \end{cases}$$

where h is a conveniently chosen threshold. The sum S_1^N is the decision function. The decision is made by using the stopping rule which is defined by

$$t_a = N \cdot \min\{K : d_K = 1\} \quad (3.54)$$

where d_K is the stopping number for the sample number K (of size N) and t_a is the alarm time. In simple words, the observation is stopped after the first sample of size N for which the decision is in favor of \mathbf{H}_1

Let us consider a typical example where the distribution is Gaussian with mean value $\mu_0 = 0$ and variance $\sigma^2 = 1$. In this example, the changing parameter is mean, and the mean after change is $\mu_1 = 4$. The probability density is given by

$$p_\theta(y) = \frac{1}{\sqrt{2\pi}} e^{-\frac{y^2}{2}} \quad (3.55)$$

and the sufficient statistic s_i is

$$s_i = \frac{\mu_1 - \mu_0}{\sigma^2} (y_i - \frac{\mu_0 + \mu_1}{2}) \quad (3.56)$$

Therefore, the decision function (3.52) is

$$S_1^N = \frac{b}{\sigma} \sum_{i=1}^N (y_i - \mu_0 - \frac{v}{2}) \quad (3.57)$$

where

$$v = \mu_1 - \mu_0 \quad (3.58)$$

$$b = \frac{\mu_1 - \mu_0}{\sigma} \quad (3.59)$$

Figure 3.10 and 3.11 show the measurements and the alarm time based on the log-likelihood ratio S_k , respectively.

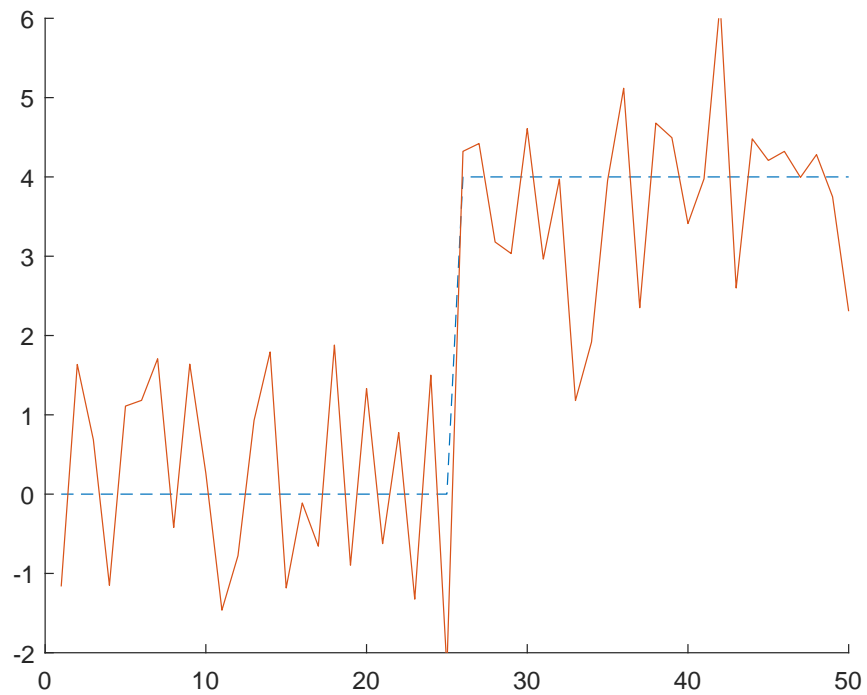


Figure 3.10: Measurements from the Gaussian distribution.

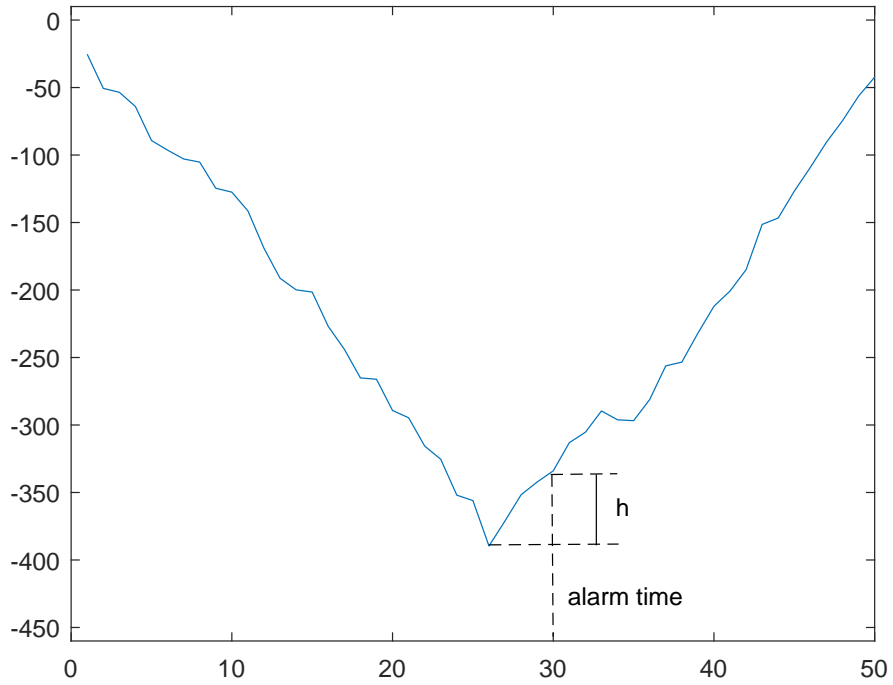


Figure 3.11: **Log-likelihood ratio s_k .** Typical behavior of the log-likelihood ratio s_k corresponding to a change in the mean.

3.2.1 CUSUM Algorithm

Now, we introduce the cumulative sum (CUSUM) algorithm, which was first proposed in 1954 [3]. There are four different derivations of CUSUM algorithm, and we only describe the more intuition-based one, which is using ideas connected to a simple integration of signals with adaptive threshold.

As we mentioned above, the typical behavior of the log-likelihood ratio S_k shows a negative shift before change, and a positive shift after change, as depicted in figure 3.11. Thus, the relevant information, as far as the change is concerned, lies in the difference between the value of the log-likelihood ratio and its current minimum value [1]; and the corresponding decision rule is that, at each time instant, to compare

this difference to a threshold as follows:

$$g_k = S_k - m_k \geq h \quad (3.60)$$

where

$$S_k = \sum_{i=1}^k s_i \quad (3.61)$$

$$s_i = \ln \frac{p_{\theta_1}(y_i)}{p_{\theta_0}(y_i)} \quad (3.62)$$

$$m_k = \min_{1 \leq j \leq k} S_j \quad (3.63)$$

Similarly, the stopping time is

$$t_a = \min\{K : g_k \geq h\} \quad (3.64)$$

and figure (3.12) shows the typical behavior of g_k . Now, it is clear that this decision rule is a comparison between the cumulative sum S_k and an adaptive threshold $m_k + h$. Because of m_k , the threshold is not only modified on-line, but also saves the complete memory of the entire information contained in the past observations.

3.3 Unknown Parameter After Change

Now, we developed a case where the parameter θ_1 after change is unknown, and the parameter θ_0 before change is still assumed to be known.

As mentioned before, the log-likelihood ratio for the measurements from time j to time k is

$$S_j^k(\theta_1) = \sum_{i=j}^k \ln \frac{p_{\theta_1}(y_i)}{p_{\theta_0}(y_i)} \quad (3.65)$$

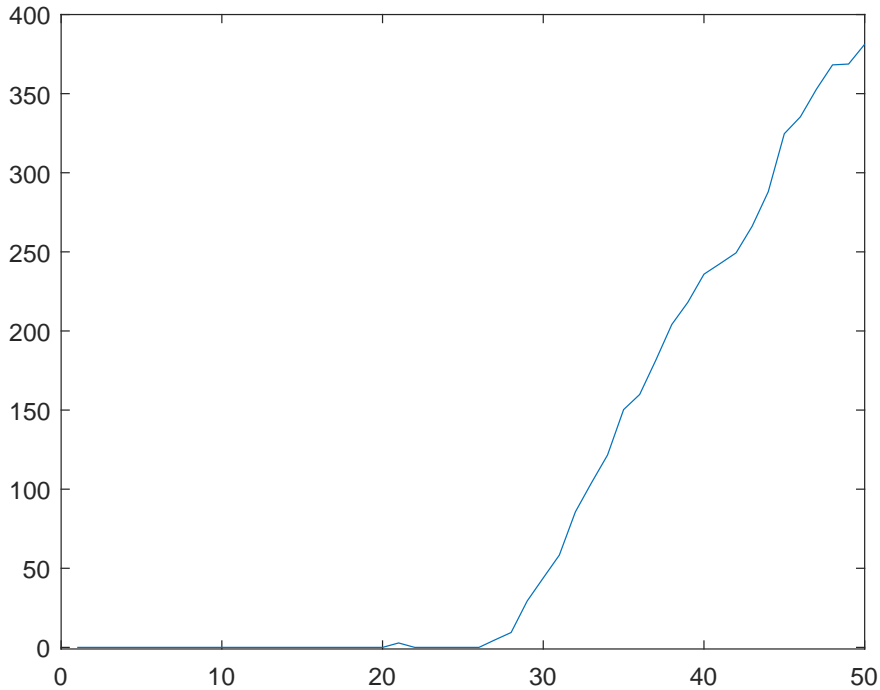


Figure 3.12: **Typical behavior of the CUSUM decision function g_k**

Now, the parameter θ_1 is unknown, and this ratio becomes a function of two unknown independent variables : the parameter θ_1 after change and the change time t_0 . The traditional statistical approach is to use the maximum likelihood estimates of these two variables, and thus the double maximization.

$$g_k = \max_{1 \leq j \leq k} \ln \hat{\Lambda}_j^k = \max_{1 \leq j \leq k} \sup_{\theta_1} S_j^k(\theta_1) \quad (3.66)$$

The detailed description of the conditions on the probability densities p_{θ_i} under which this double maximization can be performed is found in [4]. Then let us discuss if there is a priori information available about the parameter after change. In many practical problems, it is possible to obtain a minimum magnitude v_m of the changes of interest in the parameter θ_1 . In this case, the second maximization in equation (3.66) can be

changed using the magnitude v_m as follows:

$$g_k = \max_{1 \leq j \leq k} \sup_{\theta_1: |\theta_1 - \theta_0| \geq v_m > 0} S_j^k(\theta_1) \quad (3.67)$$

In such a case, we need to estimate two unknown parameters after a abrupt change has been detected : the change time t_0 and the magnitude of the jump $(\theta_1 - \theta_0)$. The conditional maximum likelihood estimates of the change time and magnitude are given by

$$(\hat{t}_0, \hat{\theta}_1) = \arg \max_{1 \leq j \leq t_a} \sup_{\theta_1: |\theta_1 - \theta_0| \geq v_m > 0} \sum_{i=j}^{t_a} \ln \frac{p_{\theta_1}(y_i)}{p_{\theta_0}(y_i)} \quad (3.68)$$

3.4 Bibliography

- [1] M. Basseville, I. V. Nikiforov, *et al.*, *Detection of abrupt changes: theory and application*, vol. 104. Prentice Hall Englewood Cliffs, 1993.
- [2] P. J. Huber and V. Strassen, “Minimax tests and the neyman-pearson lemma for capacities,” *The Annals of Statistics*, pp. 251–263, 1973.
- [3] E. S. Page, “Continuous inspection schemes,” *Biometrika*, vol. 41, no. 1/2, pp. 100–115, 1954.
- [4] G. Lorden *et al.*, “Procedures for reacting to a change in distribution,” *The Annals of Mathematical Statistics*, vol. 42, no. 6, pp. 1897–1908, 1971.

Chapter 4

Quickest Detection of Abnormal Vehicle Movements on Highways

4.1 Introduction

The drive to produce self-driving vehicle remains an active research topic over the past two decades [1] [2] [3] [4] [5]. Compared to other forms of transportation, such as aircrafts and trains, the *autonomous car* faces unique challenges: there is only a thin buffer zone between adjacent vehicles and other hazardous situation and the time to impact is in fractions of seconds. Addressing this challenge prompted intense research in the self-driving sector of the automotive industry, especially in the recent past.

Research into self-driving technology can be classified into the following categories [6] [7]:

1. *Computer vision:* The objective here is to perceive the surrounding environment by identifying objects in relevant context. Several sensors, such as Lidar [8] [9], Radar [10] [11], infrared sensors [12], ultrasound sensors [13], video cameras [14] [15] [16] [17] are used toward computer visualization of the surrounding environment.

2. *Sensor fusion*: Each self-driving vehicle is equipped with a multitude of the above mentioned sensors. For example, some self-driving prototypes have 16 radars pointing outside from all four sides of the vehicle [18]; similarly multiple video cameras collect continuous video footage from all directions [19] [20]. In almost all cases, the same information is collected by multiple sensors — this results in the challenge of information fusion: how to combine the noisy, ambiguous and distorted information that is coming from a variety of sources scattered around the vehicle body in order to get accurate and actionable knowledge? Research in sensor fusion algorithms attempt to answer this question [21].
3. *Localization*: The global positioning systems [22] (GPS) technology allows to self-localize a vehicle within centimetre accuracy [23] [24]. However, the path of a vehicle GPS often involves GPS-blackout and GPS-grey zones; localization algorithms, such as simultaneous localization and mapping (SLAM), focus on guiding the vehicle during the (intermittent) GPS-blackout/grey areas [25].
4. *Path planning*: In this phase, the vehicle decides its course of action for the next few seconds/minutes depending on the situation awareness; possible causes of actions such as accelerating/decelerating, staying the course/lane-changing, are made during path planning [26] [27]. A trajectory of possible paths are built and their safety and comfort are evaluated in this step [28].
5. *Control*: Once a path is decided, the appropriate control signal is passed through the transmission system [29] [30].

The focus of this paper is on the path planning phase. Particularly, we focus on estimating/detecting the state of surrounding vehicles as quickly as possible. Considering the proximity of surrounding vehicles and factoring in their speed, quickest detection is an important criterion for collision avoidance. This is crucial, especially when autonomous vehicles share the road with human drivers.

Collision risk has been the subject of several recent studies. The main contribution of [31] is the utilization of a naturalistic driving data set for the evaluation of collision warning / collision avoidance algorithm; here, the data is passed through a Kalman smoothing before the vehicle is classified as 'threatening' or 'safe', based on the range behaviour. The effectiveness of a rear-end collision avoidance system capable of working on both straight and curved sections of highway is studied in [32]. A real-time implementation of socially acceptable collision avoidance systems using the elastic band method for low-speed autonomous shuttle operations in high pedestrian density environments is studied in [5]. In [33], a Neural Network based approach was presented for behaviour prediction of human drivers where the effectiveness of neural network based solutions in predicting lane-changing behaviours is demonstrated through simulations. Another approach to predict and manage lane-changing behaviours is presented in [34]. Other approaches in closely related research experimented swarm intelligence [35], hidden Markov models [36], and other Bayesian approaches [37], [15].

The challenge of proximity and limited-time to actions are two defining challenges in self-driving cars. However, additional challenges abound. Most of the present day self-driving algorithms are developed and tested in favourable environments. In order to be practical, the proposed approaches need to be robust enough to deliver reliable performance in unfavourable, albeit highly probable, conditions, such as bad weather, and bad terrain. For example, the accuracy of proximity sensors such as Lidar, radar and ultrasound sensor is compromised during bad weather, e.g., winter storms. Under these circumstances, otherwise accurate measurements become highly noisy. How to make reliable decisions under these noisy scenarios? In this thesis, we answer this question in the form of a novel state-space model and a robust detector that is designed to work reliably in noisy environments.

One of the unique human abilities in driving is the ability to estimate the threat

level and to plan a response that is timely and accurate. Maneuvers, such as overtaking, lane changing, and intersection crossing are mainly evaluated according to a ratio of risk and time efficiency. There is increased attention in the scientific community to enhance the intelligence of the automation system. Any autonomous system involving mobility needs path planning; this has been the main focus in the field of autonomous control. Path planning algorithms are often described as belonging to the classical algorithms/intelligent algorithm category. The difference is that intelligent algorithms use meta-heuristics, changing conditional rules, to optimize an initial solution; on the other hand, the classical algorithms only use heuristics, fixed conditional rules, to restrict the application of the base algorithm [38]. Path-planning algorithms are evaluated based on the following priorities: completeness, optimality and time-complexity [39]. For successful and complete path planning in a cluttered environment, as the vehicle has to quickly re-plan its path, the computational time required should be less because the vehicle needs sufficient time to adjust its movement to avoid moving obstacles.

In light of the above mentioned motivations, in this thesis, we propose a novel state space model for surrounding vehicle tracking and detection of their critical states. The proposed state-space model constitutes of position and velocity in the longitudinal and lateral directions; in addition, two critical state indicators are introduced in the state-space model of each surrounding vehicle: (i) lane index (LIDX) and lane-changing-index (LcIDX). We propose an approach based on the likelihood ratio test (Page test) to have these two non-linear states up-to-date in the state-space model of each surrounding vehicle.

The remainder of this paper is organized as follows. Section 4.2 describes the applicability of proposed vehicle detection and tracking in a multi-lane, one directional highway scenario along with its vehicle motion model. Section 4.3 gives a brief theoretical background for the proposed change detection algorithm. Section 4.4 summarizes the proposed algorithm and the numerical results of it are presented

in Section 4.5. The paper is concluded in Section 4.6.

4.2 Vehicle Motion Model on Highways

Figure 4.13 shows two vehicles in a multi-lane, one-directional highway scenario where the objective of the vehicle A is to track vehicle B for collision avoidance. Let us denote the relative state of the vehicle B as

$$\mathbf{x}(k) = \begin{bmatrix} x(k) & \dot{x}(k) & y(k) & \dot{y}(k) & L_k & \dot{L}_k \end{bmatrix}^T \quad (4.69)$$

where $x(k)$ denotes the relative lateral displacement of B; $\dot{x}(k)$ denotes the relative lateral velocity of B; $y(k)$ denotes the relative longitudinal displacement of B; $\dot{y}(k)$ denotes the relative longitudinal velocity of B, $L_k \in \mathcal{I}$ denotes the lane in which the vehicle B is in, and $\dot{L}_k \in \{-1, 0, 1\}$ is another indicator function that is defined as

$$\dot{L}_k = \begin{cases} -1 & \text{B is changing its lane to the left} \\ 0 & \text{B is staying in the same lane} \\ 1 & \text{B is changing its lane to the right} \end{cases} \quad (4.70)$$

The index k denotes the samples where the sampling time, the time between sample k and sample $k - 1$, is assumed to be a constant T .

The indicators L_k and \dot{L}_k play an important part of the path planning in vehicle A. Considering that there is only limited time to take action, tracking the state of B should be done as quickly as possible.

First, let us gain some insights into the available samples of data for detection. Consider a hypothetical scenario where the vehicle B is travelling at 40 km/h (longitudinally) towards vehicle A. Assuming that the distance between them is 10 m, at 60 Hz sampling rate, there are only 54 samples available before collision. Similarly, consider another scenario where the vehicle B is travelling at 1 km/h (laterally)

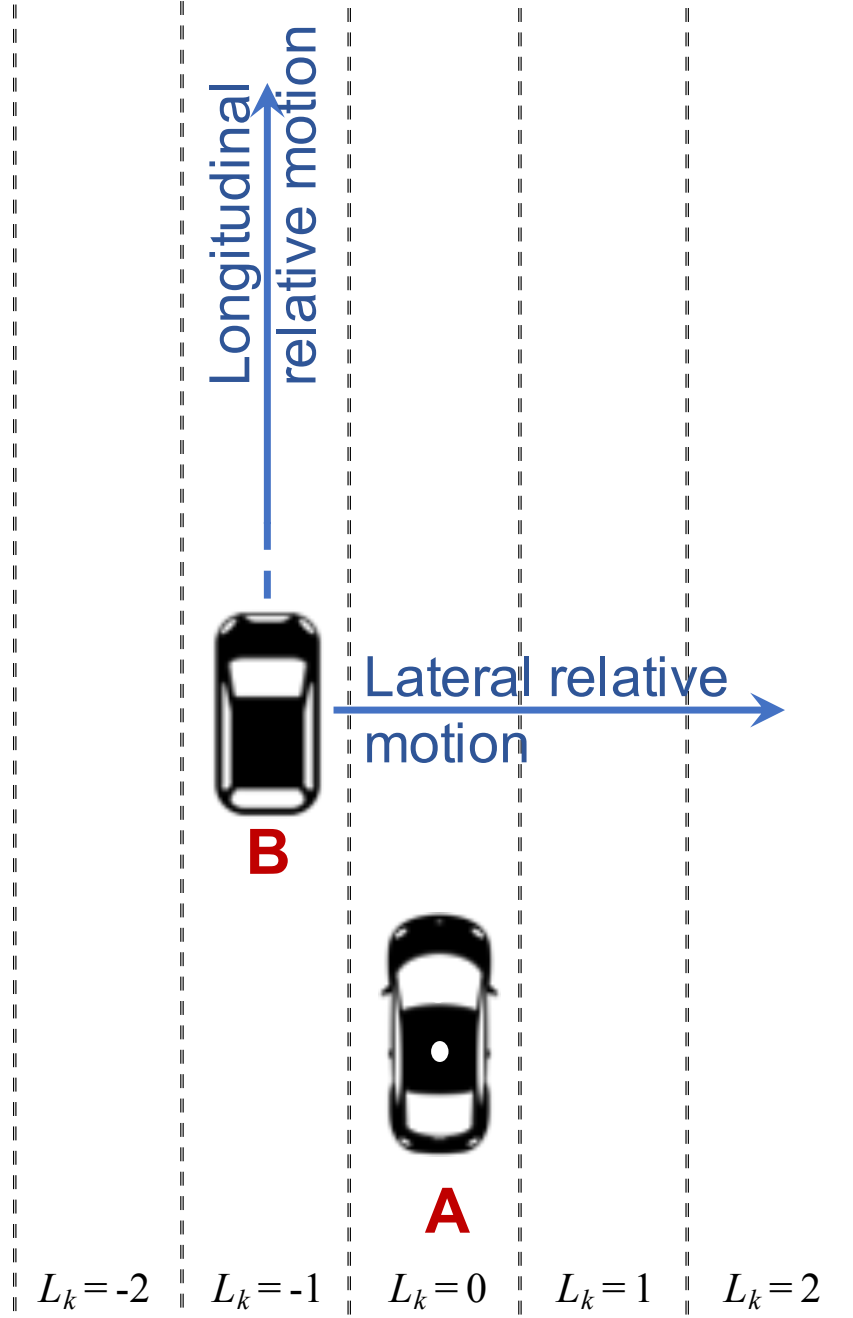


Figure 4.13: **Highway driving scenario.** Multi-lane highway scenario is depicted in this figure where vehicle A uses its sensors to track the state of vehicle B. The lane number of B is denoted by L_k , where $L_k \in [-2, -1, 0, 1, 2]$ is relative to the lane in which A is travelling.

towards the vehicle A. Assuming that the distance between them is 1 m, and at 60 Hz sampling rate, there are only 216 samples available before collision. Table 4.1 summarizes this information in order to illustrate the need to detect the state of the surrounding vehicle as quickly as possible. Hence, the required number of samples before making a decision is one of the important performance criteria of this paper.

Table 4.1: Number of Samples Before Contact (60 Hz)

	Relative Distance (m)	Relative Velocity (Km/h)	No. of Samples Before Contact
Longitudinal	10	40	54
Lateral	1	1	216

The state vector $\mathbf{x}(k)$ can be decomposed into linear and indicator (non-linear) portions as follows

$$\mathbf{x}(k) = [\mathbf{x}_l(k) \ \mathbf{x}_i(k)]^T \quad (4.71)$$

where

$$\mathbf{x}_l(k) = [x(k) \ \dot{x}(k) \ y(k) \ \dot{y}(k)]^T \quad (4.72)$$

$$\mathbf{x}_i(k) = [L_k \ \dot{L}_k]^T \quad (4.73)$$

The linear portion of $\mathbf{x}(k)$ is assumed to undergo the following process model

$$\mathbf{x}_l(k+1) = \mathbf{F}_l \mathbf{x}_l(k) + \mathbf{v}_l(k) \quad (4.74)$$

where

$$\mathbf{F}_l = \begin{bmatrix} 1 & T & 0 & 0 \\ 0 & 1 & 0 & 0 \\ 0 & 0 & 1 & T \\ 0 & 0 & 0 & 1 \end{bmatrix} \quad (4.75)$$

and process noise covariance is written as

$$E \{ \mathbf{v}_l(k) \mathbf{v}_l(k)^T \} = \begin{bmatrix} \frac{1}{3}T^3\sigma_x^2 & \frac{1}{2}T^2\sigma_x^2 & 0 & 0 \\ \frac{1}{2}T^2\sigma_x^2 & T\sigma_x^2 & 0 & 0 \\ 0 & 0 & \frac{1}{3}T^3\sigma_y^2 & \frac{1}{2}T^2\sigma_y^2 \\ 0 & 0 & \frac{1}{2}T^2\sigma_y^2 & T\sigma_y^2 \end{bmatrix} \quad (4.76)$$

where σ_x^2 is the lateral process noise variance, and σ_y^2 is the longitudinal process noise variance.

In order to track the vehicle B, the vehicle A uses a variety of sensors such as radar, lidar and video camera. Various signal and image processing algorithms are applied at these sensor outputs to get an estimate of the (x, y) position of the vehicle B to be

$$\mathbf{z}(k) = [z_x(k), z_y(k)]^T \quad (4.77)$$

Considering the estimation error involved in the above measurements, the following observation model is assumed

$$\mathbf{z}(k) = \begin{bmatrix} 1 & 0 & 0 & 0 \\ 0 & 0 & 1 & 0 \end{bmatrix} \mathbf{x}(k) + \mathbf{w}(k) \quad (4.78)$$

where the measurement noise $\mathbf{w}(k)$ accounts for the errors in processing the sensor

measurements in vehicle A. Further, it is assumed that the noise $\mathbf{w}(k)$ is zero-mean white Gaussian with covariance matrix

$$\mathbf{R} = E \{ \mathbf{w}(k) \mathbf{w}(k)^T \} = \begin{bmatrix} \sigma_{w,x}^2 & 0 \\ 0 & \sigma_{w,y}^2 \end{bmatrix} \quad (4.79)$$

Given the measurements $\mathbf{z}(k)$, the Kalman filter [40] can be employed to get the best estimates of the linear states of the vehicle B. Let us denote the KF estimate at time k to be $\hat{\mathbf{x}}_l(k|k)$ and let $\mathbf{P}_l(k|k)$ be the corresponding estimation error covariance.

4.3 Review of Quickest Detection Algorithm

4.3.1 Problem Definition

Quickest detection problem can be summarized into the following hypothesis test:

$$\begin{aligned} H_0 & : x(k) \sim P_{\theta_0} \quad 1 \leq k \leq K \\ H_1 & : x(k) \sim P_{\theta_0} \quad 1 \leq k \leq k^* - 1 \\ & \quad x(k) \sim P_{\theta_1} \quad k^* \leq k \leq K \end{aligned} \quad (4.80)$$

where the objective is to detect the instance k^* when the change in the underlying distribution of $x(k)$ occurred.

Assuming that the parameters θ_0 and θ_1 correspond to Gaussian distributions, the likelihood ratio can be written as

$$\begin{aligned} P_{\theta_0}(x(k)) &= \frac{1}{\sqrt{2\pi}\sigma_0} e^{-(x(k)-\mu_0)^2/2\sigma_0^2} \\ P_{\theta_1}(x(k)) &= \frac{1}{\sqrt{2\pi}\sigma_1} e^{-(x(k)-\mu_1)^2/2\sigma_1^2} \end{aligned} \quad (4.81)$$

The likelihood ratio between the two hypotheses can be written as

$$T_k = L_{H_1/H_0} = \ln \frac{P_{\theta_1}(x(k))}{P_{\theta_0}(x(k))} \quad (4.82)$$

which simplifies to

$$T_k = \log \left(\frac{\sigma_0}{\sigma_1} \right) + \frac{(x(k) - \mu_0)^2}{2\sigma_0^2} - \frac{(x(k) - \mu_1)^2}{2\sigma_1^2} \quad (4.83)$$

4.3.2 Batch Detection

Consider a batch of K observations. The objective is to detect if and when the change, from the null hypothesis H_0 to alternate hypothesis H_1 , if any, occurred within that batch. Assuming that the change occurred at k^* , the likelihood ratio between the hypotheses H_0 and H_1 is written as

$$\Lambda_{k^*}^K = \frac{\prod_{k=1}^{k^*-1} P_{\theta_0}(\mathbf{x}(k)) \prod_{k=k^*}^K P_{\theta_1}(\mathbf{x}(k))}{\prod_{k=1}^K P_{\theta_0}(\mathbf{x}(k))} \quad (4.84)$$

Now, (4.84) is written in the form of log-likelihood ratio as

$$S_{k^*}^K = \sum_{k=k^*}^K \ln \frac{P_{\theta_1}(\mathbf{x}(k))}{P_{\theta_0}(\mathbf{x}(k))} = \sum_{k=k^*}^K T_k \quad (4.85)$$

Hence, based on a batch of K observations, the exact time of change is detected as follows

$$\hat{k}^* = \arg \max_{1 \leq k^* \leq K} S_{k^*}^K \quad (4.86)$$

which can be obtained by searching over all K possible values of $S_{k^*}^K$.

4.3.3 Recursive Detection

Under the training based approach, we assume that both parameters $\theta_0 = \{\mu_0, \sigma_0\}$ and $\theta_1 = \{\mu_1, \sigma_1\}$ are known a priori. That is, we assume knowledge of the mean and standard deviation of the pupil diameter under each difficulty conditions. Assuming that the present corresponds to θ_0 and that the difficulty level changes to θ_1 , the objective is to quickly detect that change when it occurs based on the observations $\mathbf{x}(1), \dots, \mathbf{x}(K)$.

Assuming that the change occurred at time $k^* < K$, let us write the following log-likelihood ratio

$$S_{k^*} = \sum_{k=1}^{k^*} \ln \frac{P_{\theta_1}(x(k))}{P_{\theta_0}(x(k))} = \sum_{k=1}^{k^*} T_k \quad (4.87)$$

where S_{k^*} can be incrementally updated as new data arrives and the anomaly is declared when

$$S_{k^*} - m_{k^*} > h \quad (4.88)$$

where

$$m_{k^*} = \min_{1 \leq k \leq k^*} S_k \quad (4.89)$$

and h is a predefined threshold value.

Formally, the above anomaly detection time is written as

$$\hat{k}^* = \arg \min_{k^*} \{k^* : S_{k^*} - m_{k^*} > h\} \quad (4.90)$$

Based on the key idea from [41], (4.90) can be recursively computed as follows

$$\text{CUSUM}_k = \max \left\{ 0, \text{CUSUM}_{k-1} \right\} + T_k \quad k = 2, \dots, k^* \quad (4.91)$$

where CUSUM₀ can be initialized to 0.

4.4 Fastest Detection of Non-Linear States

In this section, we will exploit Page test that we summarized in Section 4.3 in order to derive the approaches for fast detection of lane-index (LIDX) and lane-changing-index (LcIDX). Let us also assume the availability of the up-to-date estimates of the linear state $\hat{\mathbf{x}}_l(k|k) = [x(k|k), \dot{x}(k|k), y(k|k), \dot{y}(k|k)]$ and its corresponding estimation error covariance $\mathbf{P}_l(k|k)$. Let us denote the diagonal elements of $\mathbf{P}_l(k|k)$ to be σ_x , $\sigma_{\dot{x}}$, σ_y , and $\sigma_{\dot{y}}$. Now, it can be written that

$$\begin{aligned} x(k) &\sim \mathcal{N}(x(k|k), \sigma_x) \\ \dot{x}(k) &\sim \mathcal{N}(\dot{x}(k|k), \sigma_{\dot{x}}) \\ y(k) &\sim \mathcal{N}(y(k|k), \sigma_y) \\ \dot{y}(k) &\sim \mathcal{N}(\dot{y}(k|k), \sigma_{\dot{y}}) \end{aligned} \tag{4.92}$$

4.4.1 Fastest Detection of Lane Index (LIDX)

The lane detection algorithm explained in this section needs only to be activated when the lane-change-index is in one of the two non-zero positions.

4.4.1.1 Detection to the Left

Given that the vehicle B is on lane L_k , the objective here is to detect if it has moved to lane $L_k - 1$ on the left.

$$\begin{aligned} H_0 : & \text{The vehicle B remains in lane } L_k \\ H_1 : & \text{The vehicle B has moved to lane } L_k - 1 \end{aligned} \tag{4.93}$$

i.e.,

$$\begin{aligned}
 H_0 &: x(k|k) \sim \mathcal{N}(L_k, \sigma_x) \quad 1 \leq k \leq K \\
 H_1 &: x(k|k) \sim \mathcal{N}(L_k, \sigma_x) \quad 1 \leq k \leq k^* - 1 \\
 &\quad x(k|k) \sim \mathcal{N}(L_k - 1, \sigma_x) \quad k^* \leq k \leq K
 \end{aligned} \tag{4.94}$$

where L_w denotes lane-width.

4.4.1.2 Detection to the Right

Given that the vehicle B is on lane L_k , the objective here is to detect if it has moved to lane $L_k + 1$ on the right.

$$\begin{aligned}
 H_0 &: \text{The vehicle B remains in lane } L_k \\
 H_1 &: \text{The vehicle B has moved to lane } L_k + 1
 \end{aligned} \tag{4.95}$$

i.e.,

$$\begin{aligned}
 H_0 &: x(k|k) \sim \mathcal{N}(L_k, \sigma_x) \quad 1 \leq k \leq K \\
 H_1 &: x(k|k) \sim \mathcal{N}(L_k, \sigma_x) \quad 1 \leq k \leq k^* - 1 \\
 &\quad x(k|k) \sim \mathcal{N}(L_k + 1, \sigma_x) \quad k^* \leq k \leq K
 \end{aligned} \tag{4.96}$$

4.4.2 Fastest Detection of Lane-Change Index (LcIDX)

4.4.2.1 Detection of lane change towards left

Given that the vehicle B is on lane L_k , the objective here is to detect if it is on the move to lane $L_k - 1$ on the left. This can be summarized through the following

hypothesis test

$$H_0 : \text{The vehicle B has a lateral velocity of zero} \quad (4.97)$$

$$H_1 : \text{The vehicle B has a lateral velocity of } \mu_x < 0$$

i.e.,

$$\begin{aligned} H_0 &: \dot{x}(k|k) \sim \mathcal{N}(0, \sigma_{\dot{x}}) \quad 1 \leq k \leq K \\ H_1 &: \dot{x}(k|k) \sim \mathcal{N}(0, \sigma_{\dot{x}}) \quad 1 \leq k \leq k^* - 1 \\ &\quad \dot{x}(k|k) \sim \mathcal{N}(\mu < 0, \sigma_{\dot{x}}) \quad k^* \leq k \leq K \end{aligned} \quad (4.98)$$

Here it is assumed, without loss of generality, that the hypothesis test starts at time $k = 1$.

4.4.2.2 Detection of lane change towards right

Similar to the detection of lane change towards the left, the hypothesis test reduces to the following

$$H_0 : \text{The vehicle B has a lateral velocity of zero} \quad (4.99)$$

$$H_1 : \text{The vehicle B has a lateral velocity of } \mu_x > 0$$

i.e.,

$$\begin{aligned} H_0 &: \dot{x}(k|k) \sim \mathcal{N}(0, \sigma_{\dot{x}}) \quad 1 \leq k \leq K \\ H_1 &: \dot{x}(k|k) \sim \mathcal{N}(0, \sigma_{\dot{x}}) \quad 1 \leq k \leq k^* - 1 \\ &\quad \dot{x}(k|k) \sim \mathcal{N}(\mu > 0, \sigma_{\dot{x}}) \quad k^* \leq k \leq K \end{aligned} \quad (4.100)$$

4.5 Simulation Results

The lane-changing maneuvers of the vehicle B are simulated by making use of the coordinated turn model [40]

$$\mathbf{x}(k) = \begin{bmatrix} x(k) & \dot{x}(k) & y(k) & \dot{y}(k) & \Omega_k \end{bmatrix}^T \quad (4.101)$$

where $x(k)$ denotes the relative lateral displacement of B; $\dot{x}(k)$ denotes the relative lateral velocity of B; $y(k)$ denotes the relative longitudinal displacement of B; $\dot{y}(k)$ denotes the relative longitudinal velocity of B, and Ω_k denotes the instantaneous turn rate (in degrees/sec) in which the vehicle is headed. The vehicle trajectory is simulated using the following (zero-noise) process equation

$$\mathbf{x}(k+1) = \mathbf{F}\mathbf{x}(k) \quad (4.102)$$

where

$$\mathbf{F}(\Omega_k) = \begin{bmatrix} 1 & \frac{\sin \Omega_k T}{\Omega_k} & 0 & -\frac{1-\cos \Omega_k T}{\Omega_k} & 0 \\ 0 & \cos \Omega_k T & 0 & -\sin \Omega_k T & 0 \\ 0 & \frac{1-\cos \Omega_k T}{\Omega_k} & 1 & \frac{\sin \Omega_k T}{\Omega_k} & 0 \\ 0 & \sin \Omega_k T & 0 & \cos \Omega_k T & 0 \\ 0 & 0 & 0 & 0 & 1 \end{bmatrix} \quad (4.103)$$

Figure 4.14, shows simulated vehicle trajectories for different scenarios as a line (by assuming that the vehicle remains at the center of the lane and by ignoring the vehicle dimension and showing only the center position of the vehicle). In Figure 4.14(a), the relative vehicle motion model (4.102) is used to simulate three different lane change scenarios for the vehicle B. Here, the turn angle Ω_k is kept at $\Omega_k = -45^\circ$, 0° and 45° resulting in a lane-change to the left, no lane-change and lane-change to the right, respectively.

In Figure 4.14(b), the relative vehicle motion model (4.102) is used to simulate a scenario where vehicle B overtakes A by executing the following five steps:

1. Travelling on the same lane $\Omega_k = 0^\circ$
2. Lane change move to the left with $\Omega_k = -45^\circ$
3. Travelling on the same lane $\Omega_k = 0^\circ$
4. Lane change move to the left with $\Omega_k = 45^\circ$
5. Travelling on the same lane $\Omega_k = 0^\circ$

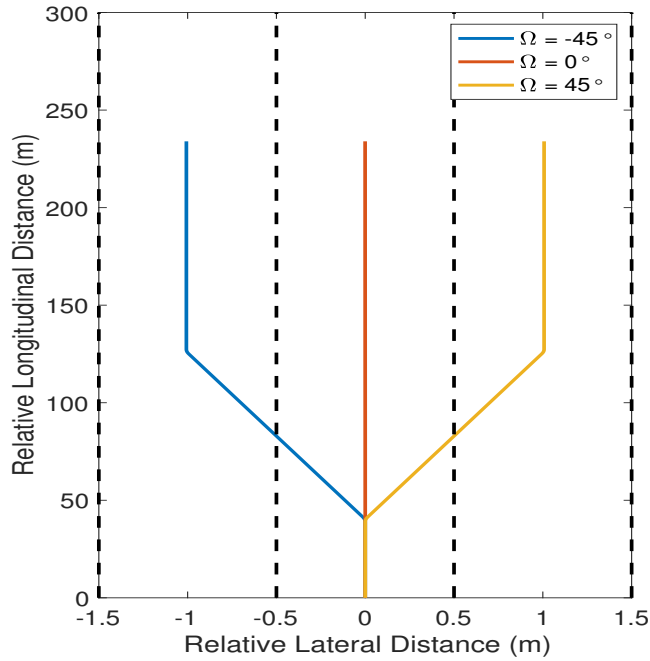
With the simulated true vehicle trajectory in (4.102), the noisy measurements are produced as follows

$$\mathbf{z}(k) = \begin{bmatrix} 1 & 0 & 0 & 0 & 0 \\ 0 & 0 & 1 & 0 & 0 \end{bmatrix} \mathbf{x}(k) + \mathbf{w}(k) \quad (4.104)$$

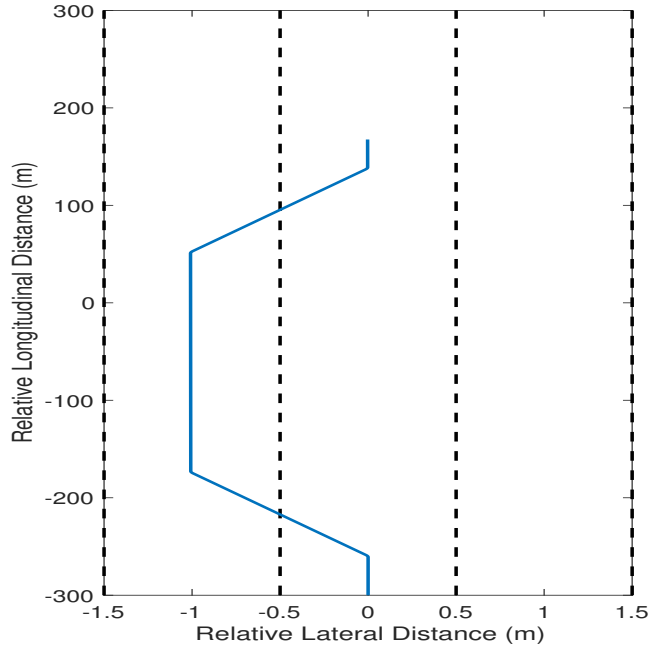
The measurement $\mathbf{z}(k)$ first goes through the Kalman filter (that employs the process and measurement models as indicated in (4.74) and (4.78)) to obtain the estimate $\hat{\mathbf{x}}(k|k)$ and the associated estimation error covariance $\mathbf{P}(k|k)$. Next, the detection algorithm described in Section 4.4 uses the estimate $\hat{\mathbf{x}}(k|k)$ in order to update the CUSUM parameters under each hypothesis discussed. Also, the detection algorithm is reset if the estimation error covariance $\mathbf{P}(k|k)$ exceeds a pre-specified threshold value.

4.5.1 Demonstration of Quickest Detection

First, we use a scenario with only one lane-changing to demonstrate the detection approach in detail. The sampling time is assumed $T = 1/32$ sec and the standard deviation of measurement noise is assumed to be $\sigma_x = 0.05$ m and $\sigma_y = 0.05$ m along



(a) Lane changing scenarios



(b) Overtake scenario

Figure 4.14: Simulated trajectories. The relative position of vehicle B is shown as it is perceived by vehicle A (see Figure 4.13). The trajectory of the vehicle center is plotted assuming that the vehicle moves along the center of the lane. The top plot shows three different lane-changing scenarios of B which was already in front of A; the plot at the bottom shows a scenario of vehicle B overtaking vehicle A.

the x and y directions, respectively. And the lateral velocity of lane-changing is assumed to be known at 0.56m/s.

Figure 4.15 shows the relative trajectory of the vehicle B as it changes lane to the left. Figure 4.16 shows the summary of Page test to detect the changing indices of LIDX and LcIDX. The noisy cartesian measurements from the sensors are shown as ‘*’ and the Kalman filter based estimated positions are also plotted as a red line on the same plot.

Figure 4.16(a) shows the detection of LIDX and Figure 4.16(b) shows the detection of LcIDX. Figure 4.16(a) illustrates that the lane-changing was precisely detected in LIDX when the lateral distance is -1 m , which is the border with the next lane. In Figure 4.16(b), LcIDX also detected the velocity change within 20 samples of actual change in a highly noisy environment. It must be mentioned that the detection algorithm is disabled when the covariance of the Kalman filter is high; this explains the absence of a false alarm at the start of the simulation – here $\mathbf{P}(k|k)$ was high due to the initialization effect of the KF algorithm.

4.5.2 Continuous Detection Algorithm

The traditional Page test is a one-way hypothesis test only. When a change towards a particular hypothesis is detected, a new test needs to be implemented in order to continuously monitor the vehicle B (i.e., LIDX and LcIDX need to be monitored continuously). Figure 4.17 shows this in the form of a state-diagram that can be used to continuously monitor vehicle B in order to detect any changes in its behaviour. The entire detection scheme always *rests* on the LcIDX detector (which operates continuously); when LcIDX detector finds that $\dot{L}_k \neq 0$, LIDX-detector becomes active in search of a lane change. After the signal $\dot{L}_k = 0$, the vehicle will stay on the current lane, and wait for the next change of signal \dot{L}_k .

Figure 4.18(b) shows the true lateral distance and the estimated distance by the

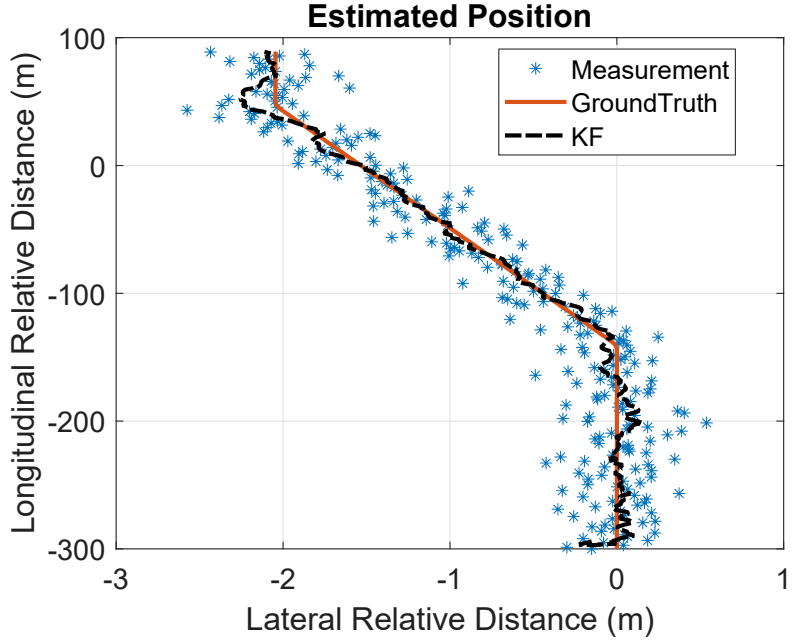


Figure 4.15: Relative trajectory of the vehicle B

Kalman filter. The page test (Section 4.4) is applied based on the KF estimates ($x(k|k)$). Once a change (from LIDX=0 to LIDX=-1) is detected is shown by '**', it means the vehicle has changed to the Lane -1. Similarly, Figure 4.18(c) shows the detection of a change (from LcIDX=0 to LcIDX=-1) is shown by **'. This detection means the vehicle is going to change to the left line (if LcIDX=-1).

4.6 Conclusions

In this thesis, we present a quickest detection approach to detect lane-changing maneuvers of a surrounding vehicle. The proposed algorithm is developed for scenarios where the measurements from otherwise reliable sensors, such as Lidar, Radar and ultrasonic sensor, become noisy due to environmental conditions. For such circumstances, we presented an approach for the optimal detection of lane-changing maneuvers of a surrounding vehicle. Our proposed solution was in the form of a novel state

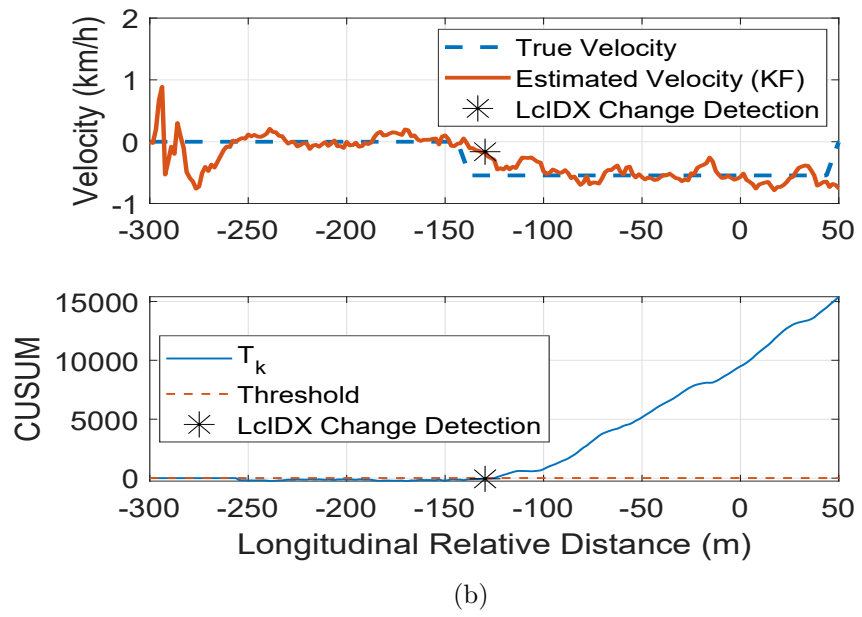
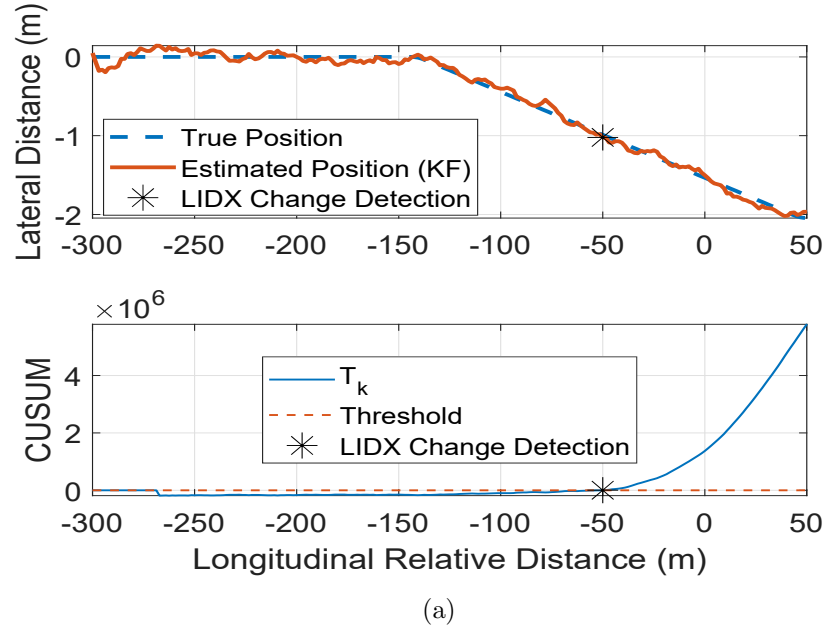


Figure 4.16: **Overtaking scenario.** Here, the relative position of vehicle B is shown as it is perceived by vehicle A (see Figure 4.13) as B overtakes A.

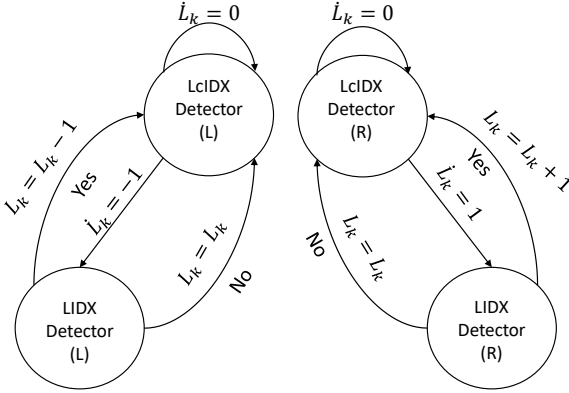
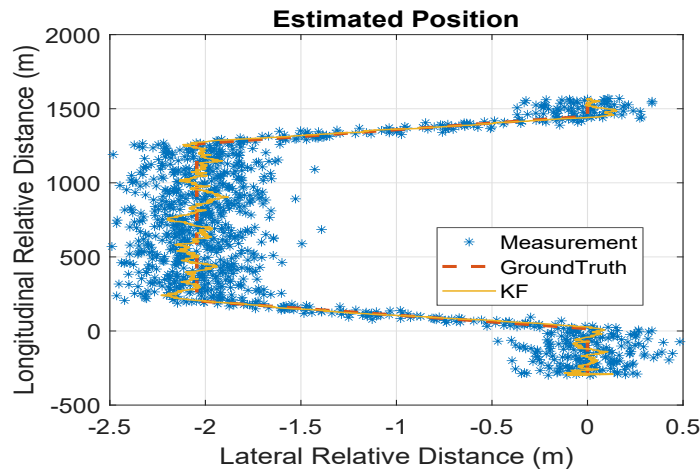
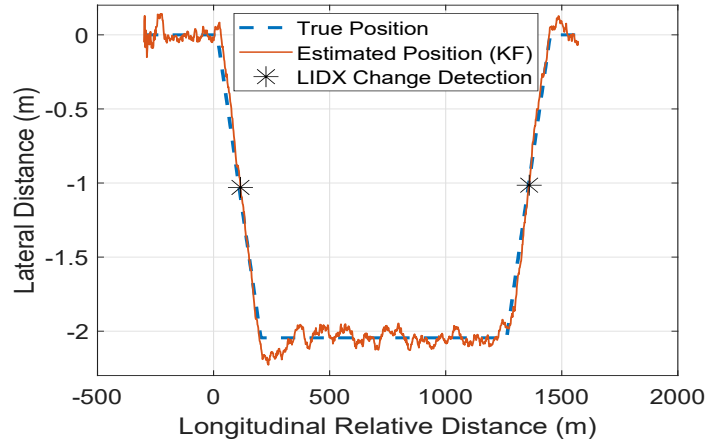


Figure 4.17: **State diagram**

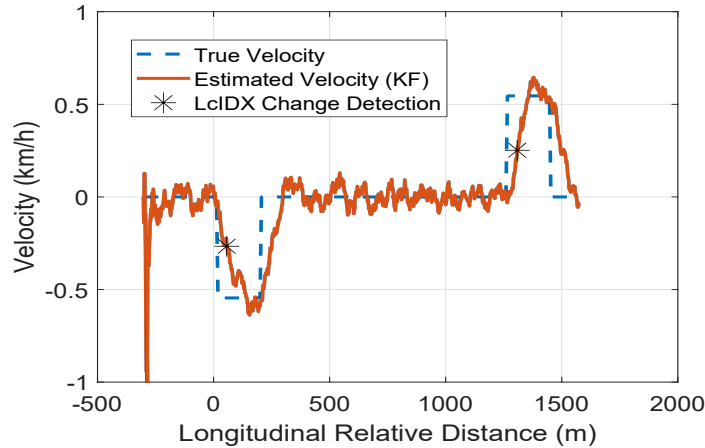
space model that includes a lane-index (LIDX) and a lane change-index (LcIDX); this paper presents the details of the optimal detector that keeps these two new indices up to date. Our future work will focus on deriving the performance bounds of the proposed detector in the form of a receiver operating characteristic (ROC) curve.



(a) Tracking vehicle trajectory using KF



(b)



(c)

Figure 4.18: **Continuous Overtaking scenario.** Here, the relative position of vehicle B is shown as it is perceived by vehicle A (see Figure 4.13) as B overtakes A, and comes back to the original lane.

4.7 Bibliography

- [1] D. Payton, “An architecture for reflexive autonomous vehicle control,” in *IEEE International Conference on Robotics and Automation*, vol. 3, pp. 1838–1845, 1986.
- [2] R. Bergholz, K. Timm, and H. Weisser, “Autonomous vehicle arrangement and method for controlling an autonomous vehicle,” Nov. 21 2000. US Patent 6,151,539.
- [3] J. Ziegler, P. Bender, M. Schreiber, H. Lategahn, T. Strauss, C. Stiller, T. Dang, U. Franke, N. Appenrodt, C. G. Keller, *et al.*, “Making bertha drive—an autonomous journey on a historic route,” *IEEE Intelligent Transportation Systems Magazine*, vol. 6, pp. 8–20, 2014.
- [4] J. Van Brummelen, M. O’Brien, D. Gruyer, and H. Najjaran, “Autonomous vehicle perception: The technology of today and tomorrow,” *Transportation research part C: emerging technologies*, vol. 89, pp. 384–406, 2018.
- [5] H. Wang, A. Tota, B. Aksun-Guvenc, and L. Guvenc, “Real time implementation of socially acceptable collision avoidance of a low speed autonomous shuttle using the elastic band method,” pp. 341–355, 2018.
- [6] S. Kato, E. Takeuchi, Y. Ishiguro, Y. Ninomiya, K. Takeda, and T. Hamada, “An open approach to autonomous vehicles,” *IEEE Micro*, vol. 35, pp. 60–68, 2015.
- [7] A. Heide and K. Henning, “the “cognitive car” a roadmap for research issues in the automotive sector,” *IFAC Proceedings Volumes*, vol. 39, pp. 44–50, 2006.
- [8] M. Bruch, “Velodyne hdl-64e lidar for unmanned surface vehicle obstacle detection,” vol. 7692, 2010.

- [9] R. W. Wolcott and R. M. Eustice, “Visual localization within lidar maps for automated urban driving,” in *RSJ International Conference on Intelligent Robots and Systems*, pp. 176–183, 2014.
- [10] S. J. Park, T. Y. Kim, S. M. Kang, and K. H. Koo, “A novel signal processing technique for vehicle detection radar,” in *MTT-S International Microwave Symposium Digest*, vol. 1, pp. 607–610, 2003.
- [11] J. Dickmann, J. Klappstein, M. Hahn, N. Appenrodt, H.-L. Bloecher, K. Werber, and A. Sailer, “Automotive radar the key technology for autonomous driving: From detection and ranging to environmental understanding,” in *IEEE Radar Conference (RadarConf)*, pp. 1–6, 2016.
- [12] T.-H. Li, S.-J. Chang, and W. Tong, “Fuzzy target tracking control of autonomous mobile robots by using infrared sensors,” *IEEE Transactions on Fuzzy Systems*, vol. 12, no. 4, pp. 491–501, 2004.
- [13] I. Ohya, A. Kosaka, and A. Kak, “Vision-based navigation by a mobile robot with obstacle avoidance using single-camera vision and ultrasonic sensing,” *Transactions on Robotics and Automation*, vol. 14, no. 6, pp. 969–978, 1998.
- [14] T. Gandhi and M. M. Trivedi, “Vehicle surround capture: Survey of techniques and a novel omni-video-based approach for dynamic panoramic surround maps,” 2006.
- [15] A. Kendall and R. Cipolla, “Modelling uncertainty in deep learning for camera relocalization,” in *IEEE international conference on Robotics and Automation (ICRA)*, pp. 4762–4769, 2016.
- [16] J. Kim and J. Canny, “Interpretable learning for self-driving cars by visualizing causal attention,” in *Proceedings of the IEEE international conference on computer vision*, pp. 2942–2950, 2017.

- [17] H. Xu, Y. Gao, F. Yu, and T. Darrell, “End-to-end learning of driving models from large-scale video datasets,” in *Proceedings of the IEEE conference on computer vision and pattern recognition*, pp. 2174–2182, 2017.
- [18] I. Bilik, O. Bialer, S. Villeval, H. Sharifi, K. Kona, M. Pan, D. Persechini, M. Musni, and K. Geary, “Automotive mimo radar for urban environments,” in *IEEE Radar Conference (RadarConf)*, pp. 1–6, 2016.
- [19] M. Bojarski, D. Del Testa, D. Dworakowski, B. Firner, B. Flepp, P. Goyal, L. D. Jackel, M. Monfort, U. Muller, J. Zhang, *et al.*, “End to end learning for self-driving cars,” *arXiv preprint arXiv:1604.07316*, 2016.
- [20] E. Santana and G. Hotz, “Learning a driving simulator,” *arXiv preprint arXiv:1608.01230*, 2016.
- [21] D. Göhring, M. Wang, M. Schnürmacher, and T. Ganjineh, “Radar/lidar sensor fusion for car-following on highways,” in *The 5th International Conference on Automation, Robotics and Applications*, pp. 407–412, 2011.
- [22] Y. Liu, X. Fan, C. Lv, J. Wu, L. Li, and D. Ding, “An innovative information fusion method with adaptive kalman filter for integrated ins/gps navigation of autonomous vehicles,” *Mechanical Systems and Signal Processing*, vol. 100, pp. 605–616, 2018.
- [23] J. Levinson, M. Montemerlo, and S. Thrun, “Map-based precision vehicle localization in urban environments.,” in *Robotics: Science and Systems*, vol. 4, p. 1, 2007.
- [24] A. de Winter and S. Baldi, “Real-life implementation of a gps-based path-following system for an autonomous vehicle,” *Sensors*, vol. 18, p. 3940, 2018.

- [25] W. Wen, L.-T. Hsu, and G. Zhang, “Performance analysis of ndt-based graph slam for autonomous vehicle in diverse typical driving scenarios of hong kong,” *Sensors*, vol. 18, p. 3928, 2018.
- [26] P. Marin-Plaza, A. Hussein, D. Martin, and A. d. l. Escalera, “Global and local path planning study in a ros-based research platform for autonomous vehicles,” *Journal of Advanced Transportation*, vol. 2018, 2018.
- [27] H. Wang, Y. Huang, A. Khajepour, T. Liu, Y. Qin, and Y. Zhang, “Local path planning for autonomous vehicles: Crash mitigation,” in *IEEE Intelligent Vehicles Symposium (IV)*, pp. 1602–1606, 2018.
- [28] S. G. Anavatti, S. L. Francis, and M. Garratt, “Path-planning modules for autonomous vehicles: Current status and challenges,” in *International Conference on Advanced Mechatronics, Intelligent Manufacture, and Industrial Automation (ICAMIMIA)*, pp. 205–214, 2015.
- [29] N. Li, D. W. Oyler, M. Zhang, Y. Yildiz, I. Kolmanovsky, and A. R. Girard, “Game theoretic modeling of driver and vehicle interactions for verification and validation of autonomous vehicle control systems,” *IEEE Transactions on control systems technology*, vol. 26, pp. 1782–1797, 2018.
- [30] R. E. Stern, S. Cui, M. L. Delle Monache, R. Bhadani, M. Bunting, M. Churchill, N. Hamilton, H. Pohlmann, F. Wu, B. Piccoli, *et al.*, “Dissipation of stop-and-go waves via control of autonomous vehicles: Field experiments,” *Transportation Research Part C: Emerging Technologies*, vol. 89, pp. 205–221, 2018.
- [31] K. Lee and H. Peng, “Evaluation of automotive forward collision warning and collision avoidance algorithms,” *Vehicle system dynamics*, vol. 43, pp. 735–751, 2005.

- [32] A. Doi, T. Butsuen, T. Niibe, T. Takagi, Y. Yamamoto, and H. Seni, “Development of a rear-end collision avoidance system with automatic brake control,” *Jsa Review*, vol. 15, pp. 335–340, 1994.
- [33] R. S. Tomar and S. Verma, “Safety of lane change maneuver through a priori prediction of trajectory using neural networks.,” *Network Protocols & Algorithms*, pp. 4–21, 2012.
- [34] A. El Hajjaji and M. Ouladsine, “Modeling human vehicle driving by fuzzy logic for standardized iso double lane change maneuver,” in *Proceedings 10th IEEE International Workshop on Robot and Human Interactive Communication*, pp. 499–503, 2001.
- [35] G. Venayagamoorthy *et al.*, “Unmanned vehicle navigation using swarm intelligence,” in *International Conference on Intelligent Sensing and Information Processing*, pp. 249–253, 2004.
- [36] C. Laugier, I. E. Paromtchik, M. Perrollaz, M. Yong, J.-D. Yoder, C. Tay, K. Mekhnacha, and A. Nègre, “Probabilistic analysis of dynamic scenes and collision risks assessment to improve driving safety,” *IEEE Intelligent Transportation Systems Magazine*, pp. 4–19, 2011.
- [37] M. Brännström, F. Sandblom, and L. Hammarstrand, “A probabilistic framework for decision-making in collision avoidance systems,” *IEEE Transactions on Intelligent Transportation Systems*, vol. 14, no. 2, pp. 637–648, 2013.
- [38] S. M. LaValle, *Planning algorithms*. Cambridge university press, 2006.
- [39] S. J. Russell and P. Norvig, *Artificial intelligence: a modern approach*. 2016.
- [40] Y. Bar-Shalom, X. R. Li, and T. Kirubarajan, *Estimation with applications to tracking and navigation: theory algorithms and software*. John Wiley & Sons, 2004.

- [41] M. Basseville, I. V. Nikiforov, *et al.*, *Detection of abrupt changes: theory and application*, vol. 104. 1993.

Chapter 5

Active RFID Based Indoor Localization

5.1 Introduction

Tracking moving objects and their localization plays a vital role for many location-based services such as livestock tracking [1], automated libraries [2], vehicle tolling [2], emergency rescuing [3]. There are many technologies that can be used for the purpose of localization and tracking such as Wi-Fi, wireless sensor networks, GPS, closed-circuit TV monitoring, etc. Real-time object tracking is a critical task in many computer vision applications such as surveillance, perceptual user interfaces, augmented reality, smart rooms, object-based video compression and driver assistance [4]. In an outdoor environment, GPS is the most promising technology to acquire the position. However, this might not be suitable for indoor localization since GPS requires a direct line of sight communication [4] [2]. GPS devices are generally not suitable to be established indoors since microwaves will be attenuated and scattered by roofs, walls and other objects. Radio frequency identification (RFID) makes indoor localization possible at a low cost. In order to achieve stride level precision radio frequency identification technology is used in the indoor positioning system.

A RFID localization system usually consists of three main components: RFID tags, RFID readers and the data processing subsystem. RFID tags can be of two types: Active and Passive tags [5]. A passive tag is an RFID tag that does not contain a battery; the power is supplied by the reader. When radio waves from the reader are encountered by a passive RFID tag, the coiled antenna within the tag forms a magnetic field. The tag draws power from it, energizing the circuits in the tag. An active RFID tag has a transmitter and its own power source. It also reads data from the tags using a defined radio frequency and protocol to transmit and receive data. The data processing subsystem utilizes the data from the reader to execute localization algorithms and make localization results available to various applications [6]. RFIDs have been widely used for human-activity tracking computer vision and active-sensor beacons [7].

Healthcare requires new technology in assisting the need of the staffs and patients. RFID localization has been an actively researched topic in the healthcare industry, driven by a greater emphasis on patient's safety than ever seen before. Primary uses of RFID in the medical sector are listed below [8] [9].

1. Monitoring physical activities of patients.
2. Tracking expensive equipment and inventory which helps in preventing human errors.
3. Tracking and monitoring patient's location, to control and document medication administration.
4. Tracking staff which helps in determining how much time staff members are actually spending with their patients, versus doing paperwork or their non-patient interaction work.

It is important for hospitals to have this information in order to effectively perform their day to day activities. In this thesis, we propose to find the received signal

strength information (RSSI) based localization approach using an active RFID system.

Before we look into the details of our approach, a few existing localization techniques are discussed. In order to improve the localization accuracy, many techniques have been proposed like LANDMARC approach, VIRE approach, ultra high frequency (UHF) RFID, unscented Kalman filter (UKF), particle filter, etc. LANDMARC is one of the most popular indoor localization technologies used in active RFID tags. The challenge is to determine an accurate indoor position using only two RFID readers with the unknown location and landmarks. The algorithm generates a map from the reference tags from known a location to locate an unknown target within the range of RFID reader [10]. In the VIRE approach of localization, to gain accurate positions, more reference tags are included, filtering out the unlikely positions. The major drawback of this method is that an appropriate threshold must be chosen as this has a tremendous effect on the performance of VIRE because the selection of threshold results in false alarms and missed detection [11]. Passive RFID is used for automated identification and data capture. Backscattered coupling and inductive coupling mechanism are used for reader to tag communication in ultra high frequency (UHF) RFID system. The RSSI is measured by measuring the backscattered radio signal. The reference tags are removed in this method of localization and a single target tag location approach is used [12]. In the reference tag technique, the locations of passive RFID tags are collected through an RFID reader that is fixed on a moving cart, that collects data from the area of interest. Passive tags are placed at a known location or reference tags. The maximum likelihood method is used to estimate the position of the target [13]. Among all localization techniques, the measurements from a cluster of heterogeneous sensors are obtained and fused. The most popular data fusion method for positioning problem is the UKF, but the computational time of the UKF is much greater than that of extended Kalman filter (EKF) [14].

In this thesis, we are interested in tracking patients in a particular room or an

area of a hospital. This method assumes that the location of k RFID readers are fixed alongside an elliptical track in a room where the patient's physical activities are to be monitored and RFID tags are attached to the patient as wearable devices who needs to be tracked. Our assumption is that all RFID readers are omnidirectional, they emit same power and all environmental conditions are taken into account as a single environmental constant c . This reduces the need for calibration which in turn reduces the computational complexity and improves the performance of localization. The reader identifies all RFID tags within its vicinity as the patients move across the track, their RSSI and the ID are stored. In order to estimate the coordinates of the patient, we implement grid-search for the initial instance, which is followed by a maximum likelihood estimation along with an extended Kalman filter. The proposed approach is developed with scalability in mind i.e, we seek to minimize personalized parameters that will make it applicable to just one facility. This paper allows the proposed RFID based personnel tracking system at an arbitrary new facility with minimum modifications.

The remainder of this paper is organized into five sections. Section 5.2 describes the problem statement along with the state and the observation model. Section 5.3 focuses on the derivations of the proposed solution. In Sections 5.4 the Cramer-Rao lower bound is derived and the simulation results are provided in Section 5.5. The paper ends with the conclusion in Section 5.6.

5.2 Problem Statement

In this section, we briefly discuss the assumption made to develop a solution for active RFID based indoor localization. Figure 5.19 shows a diagram of indoor tracks that are typical in large buildings, such as hospitals and retirement centers. The non-linear model is considered in this thesis to describe the localization of patients who move along an elliptical orbit. In this thesis, the shape of the track (ellipse in our case)

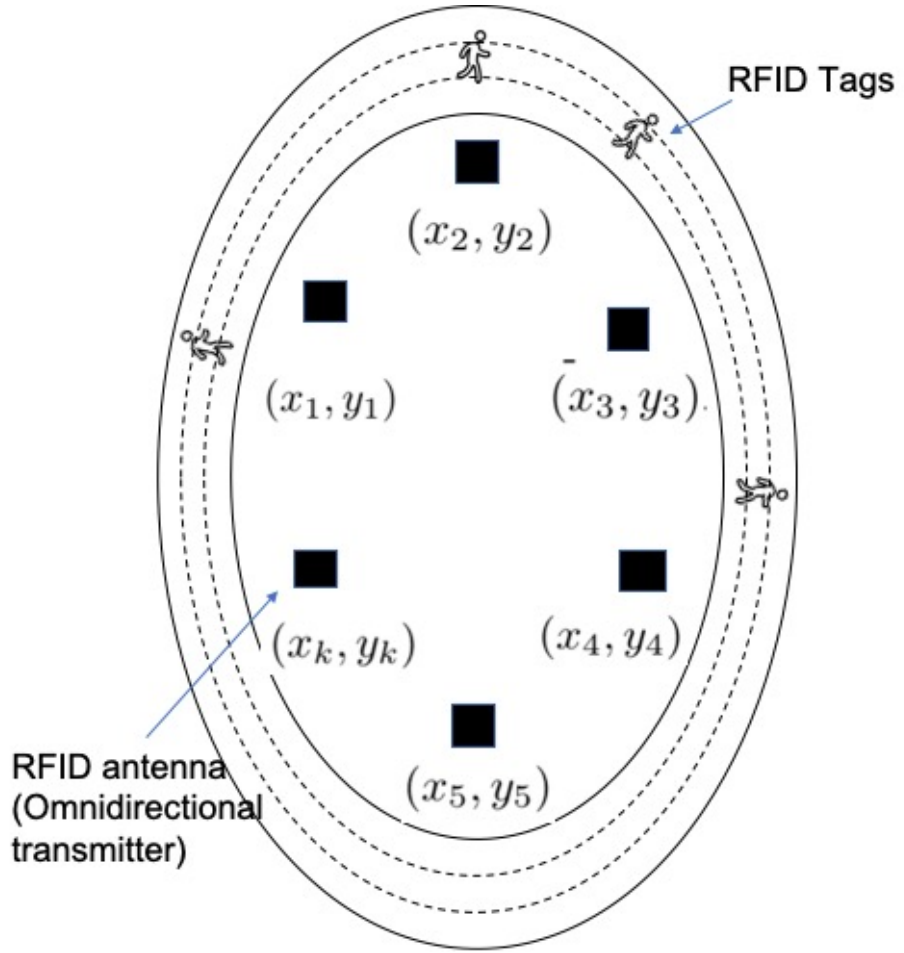


Figure 5.19: **An illustration of the problem.** Approximate positions of the RFID sensors are shown. The objective is to track the people on the tracks based on the signals received at their wearable receivers.

has no effect on the algorithms. This allows us to deploy the developed technology in different facilities without requiring any modifications. Other models can also be incorporated into the framework of an extended Kalman filter.

In the above Figure 5.19, the indoor track is assumed to be elliptical with its center at (0,0)m, semi-major axis distance as a meter and its semi-minor axis as b meter. The assumed k numbers of readers, for simplicity we assume six readers. The Cartesian position of the i th RFID reader is denoted as (x_1, y_1) , (x_2, y_2) , (x_3, y_3) , (x_4, y_4) , (x_5, y_5) . . . (x_k, y_k) .

Note: the intent of this paper is to develop a way to improve RFID localization into the tracking process, also to decide the ideal solution of the environmental constant c .

Figure 5.19 illustrates the positions of the RFID sensors and the track in which people would walk/run. It is assumed that the state (position, velocity) of the person on the track undergoes the following process model

$$\mathbf{x}(k + 1) = \mathbf{F}\mathbf{x}(k) + \mathbf{v}(k) \quad (5.105)$$

$$\mathbf{x}(k) = \begin{bmatrix} x(k) & \dot{x}(k) & y(k) & \dot{y}(k) \end{bmatrix}^T \quad (5.106)$$

where $x(k)$ is the horizontal displacement about the origin, $y(k)$ is the vertical displacement about the origin, $\dot{x}(k)$ is the horizontal velocity and $\dot{y}(k)$ is the vertical velocity.

\mathbf{F} is the state vector, given as

$$\mathbf{F} = \begin{bmatrix} 1 & T & 0 & 0 \\ 0 & 1 & 0 & 0 \\ 0 & 0 & 1 & T \\ 0 & 0 & 0 & 1 \end{bmatrix} \quad (5.107)$$

and process noise covariance is written as

$$\mathbf{Q} = E \{ \mathbf{v}(k) \mathbf{v}(k)^T \} = \sigma_w^2 \begin{bmatrix} \frac{1}{3}T^3 & \frac{1}{2}T^2 & 0 & 0 \\ \frac{1}{2}T^2 & T & 0 & 0 \\ 0 & 0 & \frac{1}{3}T^3 & \frac{1}{2}T^2 \\ 0 & 0 & \frac{1}{2}T^2 & T \end{bmatrix} \quad (5.108)$$

where σ_w^2 is the process noise variance.

Assuming there are n RFID antennas, the observation equation can be written in vector form as

$$\mathbf{z}(k) = c \begin{bmatrix} h_1(\mathbf{x}(k)) \\ h_2(\mathbf{x}(k)) \\ \vdots \\ h_n(\mathbf{x}(k)) \end{bmatrix} + \mathbf{w}(k) \quad (5.109)$$

where the i^{th} element of $\mathbf{z}(k)$ is $z_i(k)$,

$$h_i(\mathbf{x}(k)) = \frac{1}{\sqrt{(x(k) - x_i)^2 + (y(k) - y_i)^2}} \quad (5.110)$$

and the measurement noise covariance is written as

$$\mathbf{R} = E \{ \mathbf{w}(k) \mathbf{w}(k)^T \} \quad (5.111)$$

The formal statement of the problem is as follows: given the measurement vectors $\mathbf{z}(1), \mathbf{z}(2), \dots$, estimate the state $\mathbf{x}(k)$ of the person with the wearable RFID tag.

It must be noted that the observation model in (5.109) can be written as

$$\mathbf{z}(k) = \begin{bmatrix} z_1(k) & z_2(k) & \dots & z_n(k) \end{bmatrix}^T \quad (5.112)$$

where the received signal from the i^{th} RFID transmitter at time k (for a particular person) is

$$z_i(k) = \frac{c}{\sqrt{(x(k) - x_i)^2 + (y(k) - y_i)^2}} + w_i(k) \quad (5.113)$$

where $z_i(k)$ is the received signal strength at time k , (x_i, y_i) indicates the position of the i^{th} RFID antenna, $(x(k), y(k))$ indicates the position of the person on the track, $w_i(k)$ is the measurement noise that is assumed zero mean i.i.d. Gaussian with standard deviation σ_w , and environmental constant c is a constant given by [15]

5.3 Proposed Solution

5.3.1 Initialization through Maximum Likelihood Estimation

The objective here is to find a way to obtain the initial estimates of the desired states in order to initialize the EKF which will be introduced later.

First, we describe a maximum likelihood estimation (MLE) approach to estimate the position of the targets using just one measurement, $z(k)$.

Let us define the (initial) position of the target at time k as

$$\mathbf{d}(k) = \begin{bmatrix} x(k) & y(k) \end{bmatrix}^T \quad (5.114)$$

Now, $h_i(\mathbf{d}(x))$ corresponding to the i^{th} antenna can be written as

$$h_i(\mathbf{d}(k)) = \frac{1}{\sqrt{(x(k) - x_i)^2 + (y(k) - y_i)^2}} \quad (5.115)$$

The likelihood function is written as

$$\mathbf{p}(z(k)|d(k)) = \Lambda(\mathbf{d}(k)) \quad (5.116)$$

where,

$$\Lambda(\mathbf{d}(k)) = \prod_{i=1}^n \frac{1}{\sqrt{2\pi}\sigma_w} \exp \left\{ -\frac{(z_i(k) - ch_i(\mathbf{d}(k)))^2}{2\sigma_w^2} \right\} \quad (5.117)$$

Now, the ML estimate of the initial position is given by

$$\hat{\mathbf{d}}_{\text{ML}}(k) = \arg \max_{\mathbf{d}(k)} \Lambda(\mathbf{d}(k)) \quad (5.118)$$

We choose the Newton-Raphson method for this optimization. The Newton-Raphson method can be summarized as follows

$$\mathbf{d}^{j+1}(k) = \mathbf{d}^j(k) - \mathbf{D}(\mathbf{d}^j(k))^{-1} \mathbf{g}(\mathbf{d}^j(k)) \quad (5.119)$$

where $\mathbf{d}^j(k)$ is the initial position at the j^{th} iteration, and $\mathbf{D}(\mathbf{d}^j(k))$ and $\mathbf{g}(\mathbf{d}^j(k))$ are the Hessian matrix and the Jacobian vector of the likelihood function with respect to

$\mathbf{d}^j(k)$, respectively.

$$\mathbf{D}(\mathbf{d}^j(k)) = \begin{bmatrix} \mathbf{D}_{11} & \mathbf{D}_{12} \\ \mathbf{D}_{21} & \mathbf{D}_{22} \end{bmatrix} \quad (5.120)$$

$$g(\mathbf{d}^j(k)) = \begin{bmatrix} \sum_{i=1}^n \frac{-c[x^j(k) - x_i)][z_i(k) - ch_i(\mathbf{d}^j(k))][h_i(\mathbf{d}^j(k))]^3}{\sigma_w^2} \\ \sum_{i=1}^n \frac{-c[y^j(k) - y_i)][z_i(k) - ch_i(\mathbf{d}^j(k))][h_i(\mathbf{d}^j(k))]^3}{\sigma_w^2} \end{bmatrix} \quad (5.121)$$

the elements in (5.120) are given by

$$\begin{aligned} \mathbf{D}_{11} &= \sum_{i=1}^n \left\{ -\frac{\{c[\mathbf{z}_i(k) - ch_i(\mathbf{d}^j(i))][h_i^3(\mathbf{d}^j(k))]\}}{\sigma_w^2} \right. \\ &\quad + \frac{3c(x^j(k) - x_i)^2[\mathbf{z}_i(k) - ch_i(\mathbf{d}^j(k))][h_i^5(\mathbf{d}^j(k))]}{\sigma_w^2} \\ &\quad \left. - \frac{c^2(x^j(k) - x_i)^2[h_i^6(\mathbf{d}^j(k))]}{\sigma_w^2} \right\} \end{aligned} \quad (5.122)$$

$$\begin{aligned} \mathbf{D}_{12} &= \sum_{i=1}^n \left\{ \frac{3c(x^j(k) - x_i)(y^j(k) - y_i)[\mathbf{z}_i(k) - ch_i(\mathbf{d}^j(k))]}{\sigma_w^2} \times \right. \\ &\quad h_i^5(\mathbf{d}^j(k)) - \frac{c^2(x^j(k) - x_i)(y^j(k) - y_i)}{\sigma_w^2} \times \\ &\quad \left. h_i^6(\mathbf{d}^j(k)) \right\} = \mathbf{D}_{21} \end{aligned} \quad (5.123)$$

$$\begin{aligned} \mathbf{D}_{22} &= \sum_{i=1}^n \left\{ -\frac{\{c[\mathbf{z}_i(k) - ch_i(\mathbf{d}^j(k))][h_i^3(\mathbf{d}^j(k))]\}}{\sigma_w^2} \right. \\ &\quad + \frac{3c(y^j(k) - y_i)^2[\mathbf{z}_i(k) - ch_i(\mathbf{d}^j(k))][h_i^5(\mathbf{d}^j(k))]}{\sigma_w^2} \\ &\quad \left. - \frac{c^2(y^j(k) - y_i)^2[h_i^6(\mathbf{d}^j(k))]}{\sigma_w^2} \right\} \end{aligned} \quad (5.124)$$

$$(5.125)$$

The Newton's iteration also requires an initial guess $\dot{d}(k)$. We use grid search to find this initial estimation (details can be found in Section 5.5). Let us assume two

consecutive estimates of the position as

$$\hat{\mathbf{d}}_{\text{ML}}(1) = \arg \max_{\mathbf{d}(1)} \Lambda(\mathbf{d}(1)) \quad (5.126)$$

$$\hat{\mathbf{d}}_{\text{ML}}(2) = \arg \max_{\mathbf{d}(2)} \Lambda(\mathbf{d}(2)) \quad (5.127)$$

The initial velocity estimates can be obtained as

$$\begin{bmatrix} \hat{v}_x(2) \\ \hat{v}_y(2) \end{bmatrix} = (\hat{\mathbf{d}}_{\text{ML}}(1) - \hat{\mathbf{d}}_{\text{ML}}(2)) / \Delta T \quad (5.128)$$

where ΔT is the sampling time.

5.3.2 Estimate Environment Constant

Several environmental factors contribute towards the "environmental constant" denoted as c in this thesis [16]. Briefly, the constant c can be written as

$$c = \frac{P_r}{P_t} = \left[G_t g_r \left(\frac{\lambda}{4\pi d_0} \right)^2 \right] \Gamma \left[G_r g_t \left(\frac{\lambda}{4\pi d_0} \right)^2 \right] \quad (5.129)$$

where G_t and G_r are gains of the reader transmitters and antenna receivers, g_t and g_r are gains of the tag transmitters and antenna receivers, λ is the wavelength, d_0 is the distance, and Γ is the reflection coefficient.

The RFID-EKF block is summarized in Algorithm (1) and the Least Square (LS) estimate is given in (5.133). The proposed approach iterates between RFID-EKF and LS until the estimate of c converges. In this thesis, we propose a least square iterative method to estimate c . Let us define a stacked vector of N observation as

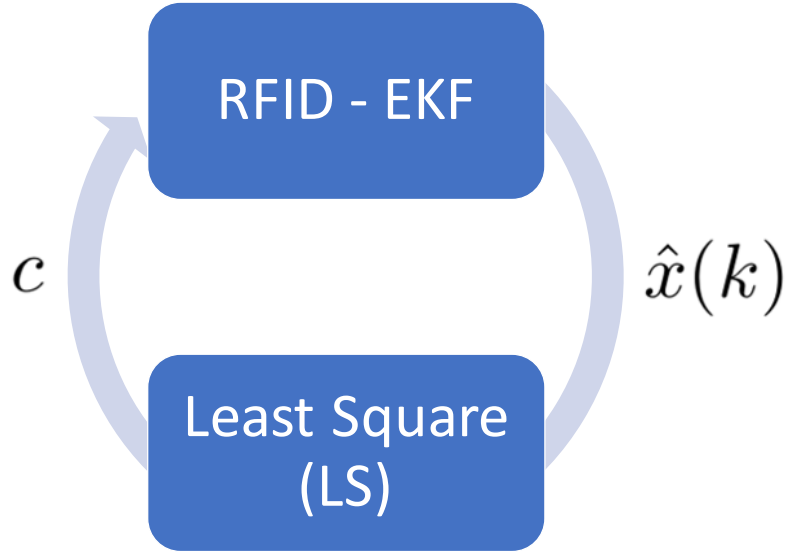


Figure 5.20: **Iterative approach to estimate the environment constant c .** The EKF is summarized in Algorithm 1 and the LS approach to estimate the constant c is summarized in (5.130)-(5.133).

$$\mathbf{z} = c \mathbf{h} + \mathbf{w} \quad (5.130)$$

which is

$$\begin{bmatrix} \mathbf{z}(1) \\ \mathbf{z}(2) \\ \vdots \\ \mathbf{z}(N) \end{bmatrix} = c \begin{bmatrix} \mathbf{h}^n(\hat{x}(1|1)) \\ \mathbf{h}^n(\hat{x}(2|2)) \\ \vdots \\ \mathbf{h}^n(\hat{x}(N|N)) \end{bmatrix} + \begin{bmatrix} w(1) \\ w(2) \\ \vdots \\ w(N) \end{bmatrix} \quad (5.131)$$

where,

$$\mathbf{h}^n(x(i)) = \begin{bmatrix} h_1(x(i|i)) \\ h_2(x(i|i)) \\ \vdots \\ h_n(x(i|i)) \end{bmatrix} \quad i = 1, 2, \dots, N \quad (5.132)$$

$$\mathbf{H}(k+1) = \begin{bmatrix} \frac{-c(x(k+1|k)-x_1))}{\sqrt{((x(k+1|k)-x_1)^2+(y(k+1|k)-y_1)^2)}}^3 & 0 & \frac{c(y(k+1|k)-y_1))}{\sqrt{((x(k+1|k)-x_1)^2+(y(k+1|k)-y_1)^2)}}^3 & 0 \\ \vdots & 0 & \vdots & 0 \\ \frac{-c(x(k+1|k)-x_n))}{\sqrt{((x(k+1|k)-x_n)^2+(y(k+1|k)-y_n)^2)}}^3 & 0 & \frac{c(y(k+1|k)-y_n))}{\sqrt{((x(k+1|k)-x_n)^2+(y(k+1|k)-y_n)^2)}}^3 & 0 \end{bmatrix} \quad (5.142)$$

and

n is the number of RFID antennas.

N is the batch number.

Then the least square estimation of c can be written as

$$\hat{c}_{LS} = (\underline{\mathbf{h}}^T \underline{\mathbf{h}})^{-1} \underline{\mathbf{h}}^T \underline{\mathbf{z}} \quad (5.133)$$

where $\hat{x}(i|i)$, $i=1, 2, \dots, N$, is defined in Section 5.3-C

5.3.3 Tracking

Based on the model described in Section 5.2, the Indoor Extended Kalman Filter tracking algorithm with 2-D map is proposed and the algorithm is shown in Algorithm 1.

5.4 Cramer-Rao Lower Bound And Posterior Cramer-Rao Lower Bound

In sub-section 5.3.1, we derived the one measurement based approach to initialize the position of the targets. In this section, we derive the Cramer-Rao lower bound [17]

Algorithm 1 $[\mathbf{x}(k+1|k+1), \mathbf{P}(k+1|k+1)] = \text{RFID-EKF}(x(k|k), P(k|k))$

Initialization:

The initialization comes from the maximum likelihood estimation in Section 5.3

State prediction:

$$\hat{\mathbf{x}}(k+1|k) = \mathbf{F}\hat{\mathbf{x}}(k|k) \quad (5.134)$$

$$\mathbf{P}(k+1|k) = \mathbf{F}\mathbf{P}(k|k)\mathbf{F}^T + \mathbf{Q} \quad (5.135)$$

Measurement prediction and residual:

$$\hat{\mathbf{z}}(k+1|k) = \mathbf{h}(\mathbf{x}(k+1|k)) \quad (5.136)$$

$$\mathbf{v}(k+1) = \mathbf{z}(k+1) - \hat{\mathbf{z}}(k+1|k) \quad (5.137)$$

Residual covariance and filter gain:

$$\mathbf{S}(k+1) = \mathbf{R} + \mathbf{H}(k+1)\mathbf{P}(k+1|k)\mathbf{H}(k+1)^T \quad (5.138)$$

$$\mathbf{W}(k+1) = \mathbf{P}(k+1|k)\mathbf{H}(k+1)^T\mathbf{S}(k+1)^{-1} \quad (5.139)$$

where $\mathbf{H}(k+1)$ is defined in equation (5.142)

Update state:

$$\hat{\mathbf{x}}(k+1|k+1) = \hat{\mathbf{x}}(k+1|k) + \mathbf{W}(k+1)\mathbf{v}(k+1) \quad (5.140)$$

$$\begin{aligned} \mathbf{P}(k+1|k+1) &= \mathbf{P}(k+1|k) - \mathbf{W}(k+1)\mathbf{S}(k+1) \\ &\quad \times \mathbf{W}(k+1)^T \end{aligned} \quad (5.141)$$

of this estimate. The one measurement based estimation error is bounded as [17]

$$E[(\hat{\mathbf{d}}(k) - \mathbf{d})(\hat{\mathbf{d}}(k) - \mathbf{d})'] \geq \mathbf{J}^{-1} \quad (5.143)$$

where the Fisher information matrix (FIM) for vector parameters $\mathbf{d}(k)$ is given by

$$\begin{aligned} \mathbf{J} &\triangleq -E\{\nabla_{\mathbf{d}(k)}\nabla'_{\mathbf{d}(k)} \ln \Lambda(\mathbf{d}(k))\}|_{\mathbf{d}(k)=\mathbf{d}(k)_0} \\ &= \begin{bmatrix} J_{11} & J_{12} \\ J_{21} & J_{22} \end{bmatrix} \end{aligned} \quad (5.144)$$

where $\mathbf{d}(k)_0$ is the true value of $\mathbf{d}(k)$. The elements of the FIM are obtained to be

$$J_{11} = \sum_{i=1}^n \frac{c^2(x(k) - x_i)^2}{\sigma_w^2[(x(k) - x_i)^2 + (y(k) - y_i)^2]} \quad (5.145)$$

$$J_{12} = \sum_{i=1}^n \frac{c^2(x(k) - x_i))(y(k) - y_i)}{\sigma_w^2[(x(k) - x_i)^2 + (y(k) - y_i)^2]} \quad (5.146)$$

$$J_{22} = \sum_{i=1}^n \frac{c^2(y(k) - y_i)^2}{\sigma_w^2[(x(k) - x_i)^2 + (y(k) - y_i)^2]} \quad (5.147)$$

$$J_{21} = J_{12} \quad (5.148)$$

Now, the CRLB is written as

$$\text{CRLB} = \mathbf{J}^{-1} \quad (5.149)$$

Next, we derive the posterior Cramer-Rao lower bound (PCRLB) [18] to compare the performance of the proposed EKF algorithm with that of the PCRLB in order to justify the use of EKF in this project. The PCRLB is bounded as [18]

$$E[(\hat{\mathbf{d}}(k|k) - \mathbf{d})(\hat{\mathbf{d}}(k|k) - \mathbf{d})'] \geq \mathbf{G}^{-1} \quad (5.150)$$

where the posterior Fisher information matrix (FIM) for vector parameters $\mathbf{d}(k)$ is given by

$$\mathbf{G}_{k+1} = \mathbf{D}_k^{22} - D_k^{21}(\mathbf{G}_k + \mathbf{D}_k^{11})^{-1}\mathbf{D}_k^{12} \quad (5.151)$$

where

$$\mathbf{D}_k^{11} = E\{-\Delta_{\mathbf{x}_k}^{\mathbf{x}_k} \ln p(\mathbf{x}_{k+1}|\mathbf{x}_k)\} \quad (5.152)$$

$$\mathbf{D}_k^{12} = E\{-\Delta_{\mathbf{x}_k}^{\mathbf{x}_{k+1}} \ln p(\mathbf{x}_{k+1}|\mathbf{x}_k)\} \quad (5.153)$$

$$\mathbf{D}_k^{21} = E\{-\Delta_{\mathbf{x}_{k+1}}^{\mathbf{x}_k} \ln p(\mathbf{x}_{k+1}|\mathbf{x}_k)\} = [\mathbf{D}_k^{12}]^T \quad (5.154)$$

$$\begin{aligned} \mathbf{D}_k^{22} &= E\{-\Delta_{\mathbf{x}_{k+1}}^{\mathbf{x}_{k+1}} \ln p(\mathbf{z}_k|\mathbf{x}_k)\} \\ &\quad + E\{-\Delta_{\mathbf{x}_{k+1}}^{\mathbf{x}_{k+1}} \ln p(\mathbf{z}_{k+1}|\mathbf{x}_{k+1})\} \end{aligned} \quad (5.155)$$

In this model, the elements \mathbf{D} can be shown as

$$\mathbf{D}_k^{11} = \mathbf{F}^T \mathbf{Q}^{-1} \mathbf{F} \quad (5.156)$$

$$\mathbf{D}_k^{12} = -\mathbf{F} \mathbf{Q}^{-1} \quad (5.157)$$

$$\mathbf{D}_k^{22} = \mathbf{Q}^{-1} + \mathbf{H}(k)^T \mathbf{R}^{-1} \mathbf{H}(k) \quad (5.158)$$

Now, the PCRLB is written as

$$\text{PCRLB} = \mathbf{G}^{-1} \quad (5.159)$$

5.5 Simulation Results

The aim of numerical simulations is to compare the performance of extended Kalman filter formulations described in the previous sections against Cramer-Rao lower bound for different values of noise standard deviation. Coordinates of the six assumed readers are taken as :

1. RFID reader 1: $(-18 \text{ m}, 9 \text{ m})$
2. RFID reader 2: $(0 \text{ m}, 9 \text{ m})$
3. RFID reader 3: $(18 \text{ m}, 9 \text{ m})$
4. RFID reader 4: $(-18 \text{ m}, -9 \text{ m})$
5. RFID reader 5: $(0 \text{ m}, -9 \text{ m})$
6. RFID reader 6: $(18 \text{ m}, -9 \text{ m})$

Figure 5.21 shows the grid map of the initial guess. The map is divided by many horizontal and perpendicular lines. The distance between two grid lines is 6m. The mean square error(MSE) of each initial method was chosen as the measure of performance. In Figure 5.22, we compare the MSE of Newton-Raphson, and grid search to CRLB. The results presented here are based on 100 Monte Carlo runs. It is evident that the MSE curve of grid search is much greater than MLE and CRLB, and the MSE curves of MLE and CRLB coincide as expected.

Figure 5.23 shows the performance of the iterative approach that was used to estimate the environmental constant c . The approach was tested for different initializations. It is found that the proposed approach to estimate the environmental constant can always converge to the true value.

Figure 5.24 shows the effect of the measurement standard deviation on the mean square error: there appears to be a quadratic relationship. The fact that PCRLB outperforms the MSE is expected since PCRLB sets a performance limit on any Bayesian

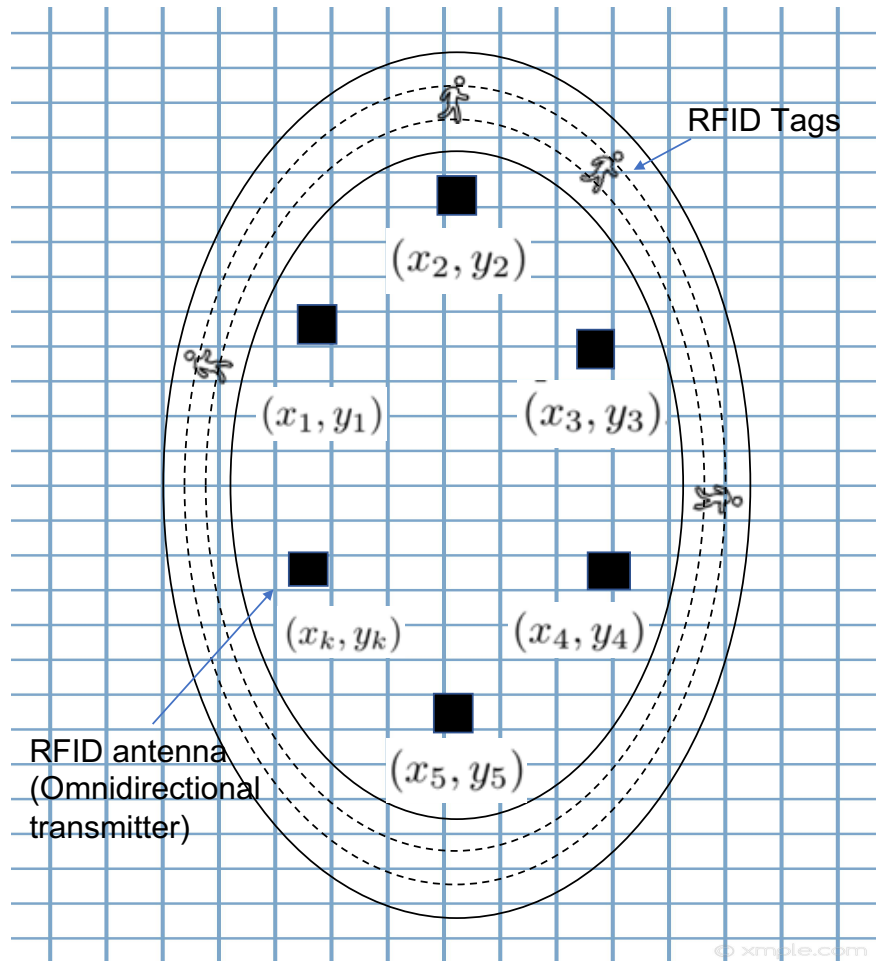


Figure 5.21: **Grid search.** Grid search is used to decide the initial guess of MLE. The search is implemented on the entire rectangular field rather than along the running path in order to ensure that the proposed technology can be portable to a new facility with fewer modifications to the algorithm.

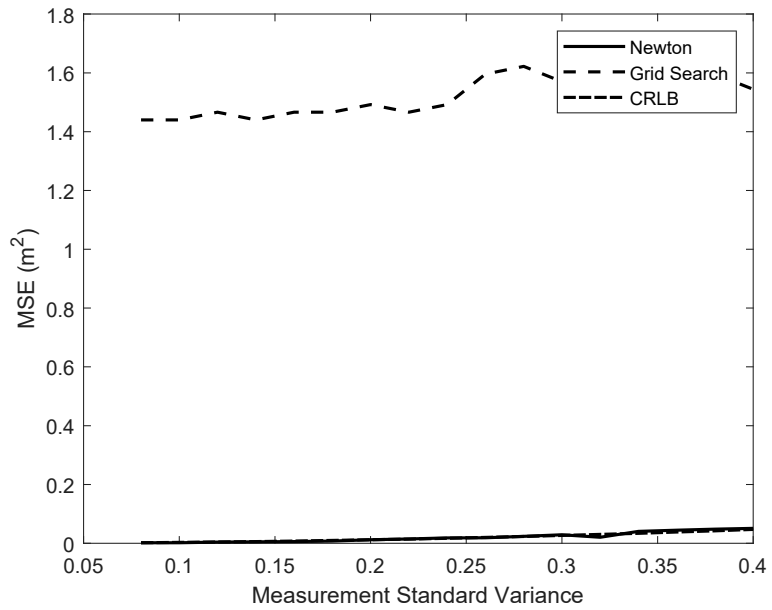


Figure 5.22: **Grid search and Newton-Raphson and CRLB.** Grid search is used to initialize the Newton-Raphson method. It is shown that the performance of the Newton-Raphson method is as good as the CRLB that was derived in (5.149).

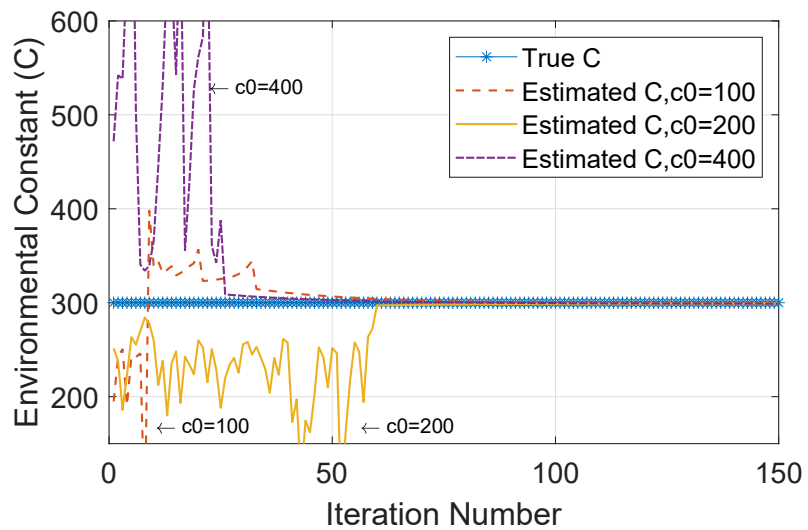


Figure 5.23: **Estimation of the environmental constant c .** The performance of estimating constant c for different initial value c_0 assumptions is shown.

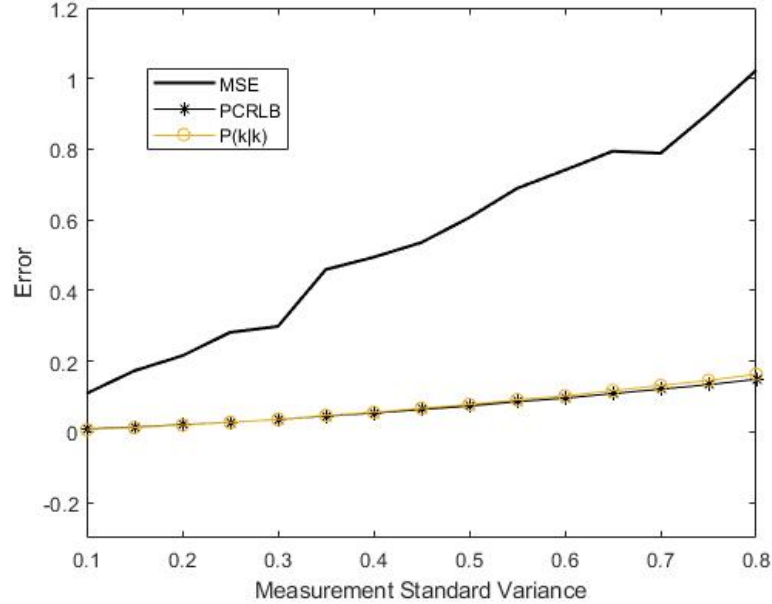


Figure 5.24: **EKF, PCRLB and $P(k|k)$** The MSE of the EKF performance is compared to PCRLB and $P(k|k)$ (5.159). It shows a clear advantage of the proposed EKF algorithm in challenging (noisy) scenarios.

estimator for the given dynamical system. Also, this figure justifies the EKF approach rather than depending on a single measurement based approach for localization. The plots in Figure 5.24 are obtained by taking the process noise standard deviation as 2 m, and the measurement noise standard deviations in the range of 0.1 to 2 for 100 Monte Carlo runs.

Figures Figure 5.25, 5.26, 5.27 and 5.28 shows the performance of the proposed RFID-EKF algorithm for indoor localization. The gray line indicates true trajectory and the black line is the estimated trajectory. These figures show the tracking performance for different measurement noise standard deviations of 0.5, 0.8, 1.2, 2.0, respectively. These figures help to visually assess the performance of the proposed scheme at varying noise levels, starting from low-noise level to very-high noise level. The performance of the proposed approach is shown to be unacceptable in high noise scenarios.

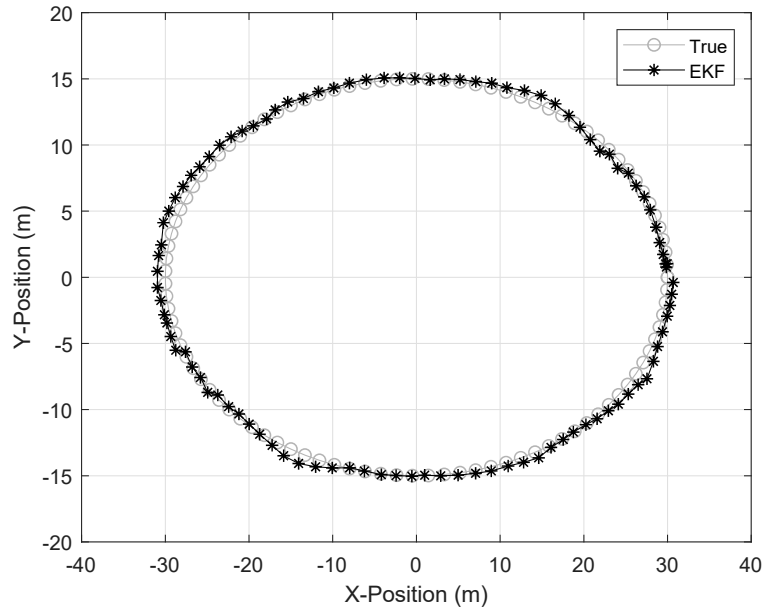


Figure 5.25: **Noise standard deviation** $\sigma_w = 0.5$. True vs. estimated trajectory at low-noise scenario.

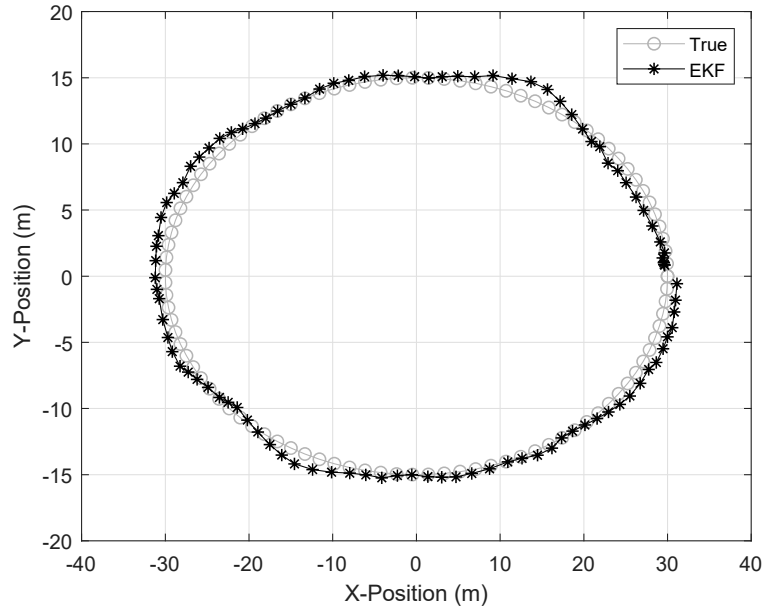


Figure 5.26: **Noise standard deviation** $\sigma_w = 0.8$. True vs. estimated trajectory for medium noise scenario.

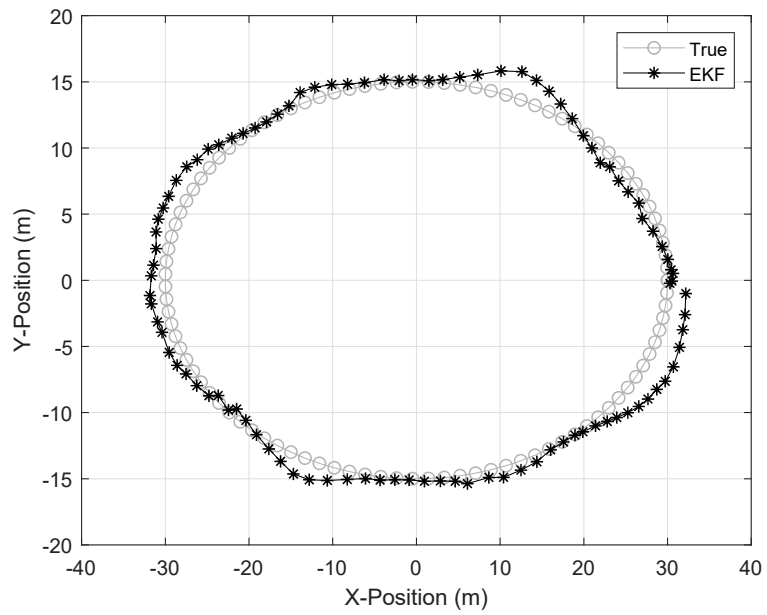


Figure 5.27: **Noise standard deviation** $\sigma_w = 1.2$. True vs. estimated trajectory is shown for a high noise scenario.

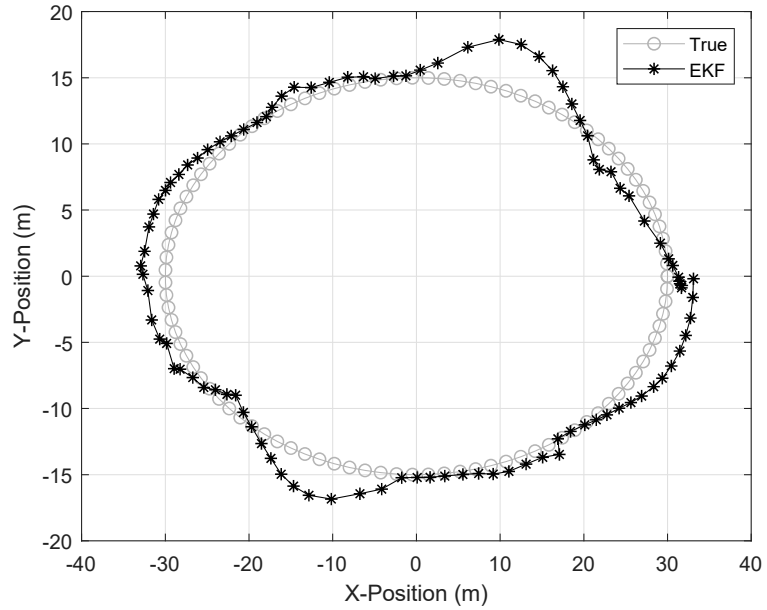


Figure 5.28: **Noise standard deviation** $\sigma_w = 2$. True vs. estimated trajectory is shown for a very-high noise scenario.

5.6 Conclusions

In this thesis, we presented an approach to track the locations of moving subjects with the help of RFID tags (that are attached to those subjects) and RFID receiving antennas. The objective of the proposed approach in this thesis is to develop an RFID based personnel and moving object tracking system with minimal requirement for “tuning” in new deployments; such a requirement seeks to limit experimental measurements, prior knowledge of possible paths and the need to calibrate for different types of environmental conditions (e.g., the distance between the RFID antenna and the surveillance region). The proposed RFID tracking scheme starts with a Newton-search to initialize an EKF based RFID tracking system; the Newton-search is initialized using a grid search. The CRLB of the initialization scheme is derived to demonstrate the advantage of the proposed EKF based tracker. In addition, an iterative parameter estimation approach, based on the least squares method, is demonstrated to estimate the environmental constant; the robustness of this scheme is demonstrated through simulation. In summary, the proposed RFID based personnel tracking scheme requires the knowledge of only the fixed RFID antennas that are to be installed to provide tracking coverage. The tracking performance of the proposed approach is found to be better than the best possible approaches that can be implemented without the use of a tracking scheme. The remaining work of this research is to conduct field testing in order to demonstrate the performance of the proposed algorithm in realistic conditions.

5.7 Bibliography

- [1] T. Balch, A. Feldman, and W. P. Wilson, “Assessment of an RFID system for animal tracking,” tech. rep., Georgia Institute of Technology, 2004.
- [2] J. L. Brchan, L. Zhao, J. Wu, R. E. Williams, and L. C. Pérez, “A real-time

RFID localization experiment using propagation models,” in *IEEE International Conference on RFID*, 2012.

- [3] S. D’Mello, E. Mathews, L. McCauley, and J. Markham, “Impact of position and orientation of RFID tags on real time asset tracking in a supply chain,” *Journal of Theoretical and Applied Electronic Commerce Research*, vol. 3, 2008.
- [4] D. Comaniciu, V. Ramesh, and P. Meer, “Kernel-based object tracking,” *IEEE Transactions on Pattern Analysis & Machine Intelligence*, 2003.
- [5] R. Tesoriero, J. A. Gallud, M. Lozano, and V. M. R. Penichet, “Using active and passive RFID technology to support indoor location-aware systems,” *IEEE Transactions on Consumer Electronics*, vol. 54, 2008.
- [6] L. M. Ni, D. Zhang, and M. R. Souryal, “RFID-based localization and tracking technologies,” *IEEE Wireless Communications*, vol. 18, 2011.
- [7] J. R. Smith, K. P. Fishkin, B. Jiang, A. Mamishev, M. Philipose, A. D. Rea, S. Roy, and K. Sundara-Rajan, “RFID-based techniques for human-activity detection,” *Communications of the ACM*, vol. 48, 2005.
- [8] J. Cho, S. Cobbs, E. Curtiss, K. Overton, and M. Redner, “Use of RFID in healthcare industry,” *Acad. Bus. Res. Inst*, 2013.
- [9] S.-W. Wang, W.-H. Chen, C.-S. Ong, L. Liu, and Y.-W. Chuang, “RFID application in hospitals: a case study on a demonstration RFID project in a taiwan hospital,” in *Proceedings of the 39th Annual Hawaii International Conference on System Sciences*, 2006.
- [10] B. Hu, H. Peng, and Z. Sun, “LANDMARC localization algorithm based on weight optimization,” *Chinese Journal of Electronics*, vol. 27, 2018.

- [11] Y. Zhao, Y. Liu, and L. M. Ni, “Vire: Active RFID-based localization using virtual reference elimination,” in *International Conference on Parallel Processing*, 2007.
- [12] J. S. Choi, H. Lee, R. Elmasri, and D. W. Engels, “Localization systems using passive UHF RFID,” in *Fifth International Joint Conference on INC, IMS and IDC*, 2009.
- [13] S. Siachalou, A. Bletsas, J. Sahalos, and A. G. Dimitriou, “RSSI-based maximum likelihood localization of passive RFID tags using a mobile cart,” in *IEEE Wireless Power Transfer Conference*, 2016.
- [14] M. St-Pierre and D. Gingras, “Comparison between the unscented Kalman filter and the extended Kalman filter for the position estimation module of an integrated navigation information system,” in *IEEE Intelligent Vehicles Symposium*, pp. 831–835, 2004.
- [15] A. Bekkali, H. Sanson, and M. Matsumoto, “RFID indoor positioning based on probabilistic RFID map and kalman filtering,” in *IEEE International Conference on Wireless and Mobile Computing, Networking and Communications*, 2007.
- [16] T. S. Rappaport *et al.*, *Wireless communications: principles and practice*, vol. 2. prentice hall PTR New Jersey, 1996.
- [17] Y. Bar-Shalom, X. R. Li, and T. Kirubarajan, *Estimation with applications to tracking and navigation: theory algorithms and software*. John Wiley & Sons, 2004.
- [18] P. Tichavsky, C. H. Muravchik, and A. Nehorai, “Posterior cramér-rao bounds for discrete-time nonlinear filtering,” *IEEE Transactions on signal processing*, vol. 46, 1998.

Chapter 6

Conclusion and Future Work

Safety and reliability are the most important properties in autonomous driving field. The strict reliability and safety requirements are critical for human safety and to help drive social acceptance of the nascent self-driving technology. In this thesis, first, we present the Page Test algorithm to detect the lane-changing behavior under high noise condition. After that, we demonstrate a radio frequency identification (RFID) indoor localization tracking algorithm based on extended Kalman filter (EKF). However, all of the test results are from computer simulation, which means our algorithm may not work effectively with the real world data. In the future, we look forward to collecting some real data or use the public datasets and adjust our algorithms to be adapted to the real environment.

Vita Auctoris

NAME:	Jingyu Wang
PLACE OF BIRTH:	Fushun, Liaoning, China
YEAR OF BIRTH:	1994
EDUCATION:	No. 2 High School , Fushun, Liaoning, China 2009-2012
	Xi'an Jiaotong University, Xi'an, Shaanxi, China 2012-2016, Bachelor of Science Mechanical Engineering
	University of Windsor, Windsor, Ontario, Canada 2017-2019, Master of Applied Science Electrical and Computer Engineering